Contents

List of Figures

List of Tables

List of symbols

$\boldsymbol{d}$, $\boldsymbol{d}_c$, $\boldsymbol{\varphi}$, $\boldsymbol{\varphi}_c$	Global and corotational displacements and rotations
$\boldsymbol{d}_e$, $\boldsymbol{d}_{ce}$	Vectors that collect both displacements and rotations element-wise
$\boldsymbol{g}[\boldsymbol{d}_e]$	Linear displacement in corotational frame geometrically dependent on global displacement
$\Phi_e[u]$	Mixed Hellinger–Reissner energy functional
u	Unknowns of the mixed functional dependent of two fields: stresses and displacements
$u(x,y),\ v(x,y)$	Continous displacement and
$w(x,y),\ \theta(x,y)$	rotational fields
$\theta(x,y),\ \theta(x,y)$	
$\boldsymbol{S}[\boldsymbol{u}_1]$	Second energy variation in vector format
$\boldsymbol{s}[\boldsymbol{u}_1, \boldsymbol{u}_2]$	Third energy variation in vector format

Chapter 1

Introduction

In the reviews of numerical methods used in nonlinear FE analysis
[1], Riks identified two main approaches: the so–called *path–following*
and the *asymptotic* analysis. Both apply to a structure subjected to
an assigned loading path, usually in the form of a proportional static
loading, which is described by defining its potential energy in terms
of a discrete set of parameters, all collected into a *configuration vector*
through the assumed FE interpolation.

The relationship between the configuration vector and the load mul-
tiplier defining a curve (maybe composed of several separate branches)
usually called *equilibrium path*. The aim of the analysis will be that of
obtaining an accurate evaluation of its natural branch.

The basic idea in the path–following approach is to recover the equi-
librium path by determining a sequence of equilibrium points suffi-

ciently near to allow the equilibrium curve to be obtained by interpolation. The analysis develops into a step-by-step process. In each step, the new equilibrium point is determined, starting from an attempt value of the next equilibrium point generally obtained by an extrapolation from the previous step (Predictor), by an iterative Newton–Raphsson scheme which provides a convergent sequence of correction to the first attempt (Corrector), thus allowing to reduce the equilibrium error within an acceptable tolerance.

Different schemes have been proposed in literature to perform the iteration, but all of them appear as minor variations of the *arc–length scheme* originally proposed by Riks in [2]. A well know variant use a non linear extrapolation [3].

The main feature of the arc-length scheme is that it provides a simple way to overcome limit points because the extended system remains not singular even if the Hessian becomes singular. This was a real difficulty before the 1979 Riks' paper.

To be noted that path–following analysis only needs the response vector, that is the first variation of the strain energy, to be evaluated accurately, being directly related to the equilibrium check. Conversely, the same accuracy is not actually needed for the second variation of the energy which provides the Hessian matrix because this matrix is only used as a part of the iteration process and its accuracy only influences the convergence of the process. A fairly rough approximation is

generally sufficient for this purpose.

As a consequence, if using small steps and an appropriate configuration updating able to reduce, as much as possible, geometrical incoherencies and avoid objectivity errors which could accumulate in the iterative process, the accuracy demand in the nonlinear modeling can be noticeably reduced .

The asymptotic analysis essentially corresponds to the implementation of Koiter's approach to nonlinear elastic stability [4] into a general FE context and the solution process is based on an expansion in Taylor's series of the potential energy, which is characterized by fourth–order accuracy.

The actual implementation of the asymptotic approach as a computational tool is therefore remains of the order of that required by a standard linearized multi–modal stability analysis.

Also if the path-following strategy is a powerful approach to the postbuckling analysis of slender elastic structures [2], however it only aimes to provide the response for a single loading case, while a global evaluation of structural collapse safety, which is our principal aim, should consider all possible loadings including the deviations due to load imperfections and geometrical defects. As the single analysis is computationally quite expensive, performing a complete investigation to consider all possible imperfection shapes is difficult. Then the asymptotic approach could be a convenient alternative for this purpose by

providing an effective and reliable strategy for predicting the initial post–critical behavior in both cases of limit or bifurcation points. Its main advantage lies in the possibility of performing an efficient and robust imperfection sensitivity analysis even in cases of multiple, nearly coincident, buckling loads.

In fact, it provides the initial post–buckling behavior of the structure, including *modal interactions* and *jumping–after–bifurcation* phenomena. Moreover, the presence of small loading imperfections or geometrical defects can be taken into account with a negligible computational extra–cost, thus allowing an inexpensive imperfection sensitivity analysis (e.g see [5, 6]).

Furthermore, we can also extract information about the worst imperfection shapes [7, 8] we can use to improve the imperfection sensitivity analysis or for driving more detailed investigations through specialized path–following analysis [9].

While being less diffuse than path–following approaches within computational mechanics (maybe because of its high demands in terms of modeling accuracy)

The asymptotic approach is based on a fourth–order expansion of the strain energy. Thus, a careful tuning of both the continuum model and its finite element implementation is needed, to obtain accurate results, and a coherent evaluation of the kinematical relationship, at least until the fourth–order strain energy variations, is necessary [10].

This is an unusual requirement (path–following analysis only needs second–order accuracy for recovering the elastic response vector and the tangent stiffness matrix when a corotational or updated Lagrangian description is used), but it is important for the reliability of the results , particularly in cases where the buckling is not followed by a significant stress redistribution [11]. Geometrically exact (or, at least, fourth–order accurate) strain models are generally too complex to be used in FEM analysis or are unavailable. Conversely, current modelings, based on technical simplifications, fail to represent the strain energy as uninfluenced by rigid motions, which is an essential objectivity requirement for the analysis. To overcome this difficulty, an external tool able to provide a coherent, fourth–order accurate, description of the rigid motion of the element is needed. The corotational approach (CR) [12, 13] appears to be suitable for this goal and will be exploited in this work.

A general strategy to recover objective nonlinear structural FE models based on corotational description and aimed to Koiter asymptotic approach has been discussed in the paper [14]. The corotational description has been used as a general tool to satisfy the objectivity requirement by referring each element to a local frame which moves (rotates) with the element, thus filtering its rigid motion. In this description, the nonlinearity of the problem derives essentially from the change of reference, from the global fixed frame to the local one, the

strain energy being governed by their relative rotations. The great advantage of the method consists in the discretization phase of the process. The construction of the FE model, for the smallness of the displacements and rotations in the corotational frame, is the same of the linear elastic case, with great advantage in term of simplicity and of reuse of standard FE library. The main difficulty is in the determination of the relationship between finite element parameters in the corotational frame and the corresponding quantities in the fixed global frame. In particular, in finite kinematics the presence of finite rotations noticeably complicates the algebra for obtaining kinematics expressions.

Frame invariance in the element definition can be recovered by referring the interpolation to a corotational framing moving with the element in such a way to filter its rigid rotation. This approach, we call *corotational interpolation*, has been discussed in detail in [14].

It is worth mentioning that a mixed extrapolation is generally convenient to avoid the so called nonlinear locking phenomena [15–17], so configuration u, used in the previous equation, usually collects both displacements and stresses.

The use of a mixed format such as that described in eqs. (1)–(4), where stresses are defined separately and determined numerically directly exploiting equilibrium equations, avoids this interaction and noticeably improves the convergence without any need to decrease the

step length more than strictly required for an accurate description of the equilibrium path (see [17], for a detailed discussion).

Within an asymptotic approach, coupled with a mixed FEM representation in stress–displacement variables [16], the overall picture changes. All quantities which define the configuration state are obtained through a direct extrapolation, thereby reducing or completely eliminating, the need for an updating process. Nonetheless, we need an accurate evaluation for the first four variations of strain energy. The paper fouses on this goal which is reached by referring to a vectorial parametrization of the rotation [**?**, **?**] and deriving explicit expressions for the first four derivatives of the corotational transformation. When combined with a second order accurate local description of the strain energy, this allows a rather simple evaluation of the required energy variations which is completely free from both extrapolation and interpolation locking [**?**]. To show the effectiveness of the proposed approach, it was implemented in a simple case of assemblages of 3D Reissner beams. This context was chosen because it both allows an easy comparison with reference "exact" results and, due to the low stress redistribution in the postbuckling range, is very sensitive to the objectivity of the strain energy description and thus convenient for checking the potential accuracy of the approach.

The work is organized as follows: after this brief introduction in the problem a presentation of the general features of Koiter's asymptotic

analysis (chapter 2) also is given a short review of 3D rotation algebra.

The energy variations, based on a corotational description are derived (chapter 3) and a complete description of the procedure needing to obtain a general and element independent framework for the Koiter's analysis is given.

In order to show how a new finite element can be casted in the Koiter's framework an high-performance shell finite element is described (chapter 4). This element is based on a mixed stress formulation and with a good behavior in the linear/elastic case. Here, a quadrilateral 4-node finite element (6 displacement dofs per node) is used. In particular, a displacement scheme, involving the Allman drilling rotations, is used for the in-plane behavior ([**?**, **?**]), as well as a linked displacement interpolation is used for the out-plane behavior (see [**?**, **?**] suitable also for thick plate analysis. The stress resultants approximation is ruled by the minimum number of parameters, both for the in-plane and the out-plane part.

The casting in to nonlinear asymptotic framework is showed (chapter 5) by only identifying the local variables whit the global ones and by choosing a suitable corotational frame reference fo the element.

Several numerical results are presented and discussed (chapter 6) showing the effectiveness and robustness of the proposed approach. In particular, the accuracy in reproducing the nonlinear equilibrium path in both cases of monomodal and coupled multimodal buckling is shown

by comparison with the commercial code ABAQUS [**?**] and the asymptotic code KASP [**?**].

Finally, a conclusive discussion (chapter 7) about the work, the results and about the possible topics for further research is reported.

Chapter 2

The Koiter's asymptotic numerical method

It has been described in detail in many papers (e.g. see [?,?,5,11,16–29] and references therein), thus it only needs to be briefly summarized here. Note that this approach can provide a very accurate recovery of the equilibrium path, as it derives from both numerical testings and theoretical investigations (e.g. Brezzi and al. [?], by discussing the simplest version of the method described in [?], derived an error estimate of $\mathcal{O}[\xi^5]$ for the limit load value). Conversely, it makes great use of information attained from a 4th–order expansion of the strain energy and then requires a 4th–order accuracy be guaranteed in the structural modeling in order to obtain an appropriate evaluation of each term of the expansion. Even small inaccuracies in this evaluation, de-

riving from geometrical incoherencies in the higher–order terms of the expansion of the $\varepsilon[d]$ law or in its finite element representation, significantly affect the accuracy or the solution and can make it unreliable. It is also very sensitive to the format used in the extrapolation, to avoid *extrapolation locking* (see **[?]** for a discussion about this topic), and the use of a mixed equation format is generally needed to obtain a robust implementation.

2.1   Outline on numerical formulation

We consider a slender hyperelastic structure subject to conservative loads $\lambda \hat{p}$ increasing with the amplifier factor λ. The equilibrium is expressed by the virtual work equation:

$$\Phi'[u]\delta u - \lambda \hat{p} \delta u = 0 \; , \; \forall \, \delta u \in \mathcal{T} \tag{2.1}$$

where $u \in \mathcal{U}$ is the field of configuration variables, $\Phi[u]$ denotes the strain energy, $\mathcal{T}$ is the tangent space of $\mathcal{U}$ at u and a prime is used for expressing the Frechèt derivative with respect to u. We assume that $\mathcal{U}$ will be a linear manifold so that the space of virtual displacements $\mathcal{T}$ will be independent of u.

Eq.(2.1) defines a curve in the (u, λ) space, the *equilibrium path* of the structure, that can be composed of several branches. We are usually interested in the branch starting from an initial known equilibrium

point $\{u_0, \lambda_0\}$ and without any loss of generality we can consider $u_0 = 0$, $\lambda_0 = 0$.

The asymptotic method provides an approximation of the equilibrium path by performing the following steps:

1. The *fundamental path* is obtained as a linear extrapolation, from a known equilibrium configuration:

$$u^f[\lambda] := \lambda \hat{u} \tag{2.2}$$

where $\hat{u}$ is the tangent evaluated at $\{0, 0\}$, obtained as a solution of the linear equation

$$\Phi''_0 \hat{u} \delta u = \hat{p} \delta u , \quad \forall \delta u \in \mathcal{T} \tag{2.3}$$

and a pedex denotes the point along u^f which the quantities are evaluated, that is $\Phi''_0 \equiv \Phi''[u^f[\lambda_0]]$.

2. A cluster of buckling loads $\{\lambda_1 \cdots \lambda_m\}$ and associated buckling modes $(\dot{v}_1 \cdots \dot{v}_m)$ are defined along $u_f[\lambda]$ by the critical condition

$$\Phi''[u^f[\lambda_i]]\dot{v}_i \delta u = 0 , \quad \forall \delta u \in \mathcal{T} \tag{2.4}$$

Buckling loads are considered to be sufficiently close to each other to allow the following linearization

$$\Phi''_b \dot{v}_i \delta u + (\lambda_i - \lambda_b)\Phi'''_b \hat{u} \dot{v}_i \delta u = 0 , \quad \forall \delta u \in \mathcal{T} \tag{2.5}$$

λ_b being an appropiate reference value of λ (e.g. the first of λ_i or their mean value). Normalizing we obtain $\Phi_b''' \hat{u} \dot{v}_i \dot{v}_j = -\delta_{ij}$, where δ_{ij} is Kroneker's symbol.

3. The tangent space $\mathcal{T}$ is decomposed into the tangent $\mathcal{V} \equiv \{\dot{v} = \sum_i \xi_i \dot{v}_i\}$ and orthogonal $\mathcal{W} \equiv \{w : \Phi_b''' \hat{u} \dot{v}_i w = 0\}$ subspaces so that $\mathcal{T} = \mathcal{V} \oplus \mathcal{W}$. Making $\xi_0 = \lambda$ and $\dot{v}_0 := \hat{u}$, the asymptotic approximation for the required path is defined by the expansion

$$u[\lambda, \xi_k] \equiv \sum_{i=0}^m \xi \dot{v}_i + \frac{1}{2} \sum_{i,j=0}^m \xi_i \xi_j w_{ij} \tag{2.6}$$

where w_{ij} are quadratic corrections introduced to satisfy the projection of eq.(2.1) onto $\mathcal{W}$ and obtained by the linear *orthogonal equations*

$$\Phi_b'' w_{ij} \delta w = -\Phi_b''' \dot{v}_i \dot{v}_j \delta w \ , \ w_{ij}, \delta w \in \mathcal{W} \tag{2.7}$$

where, due to the orthogonality condition, $w_{0i} = 0$.

4. The following energy terms are computed for $i, j, k = 1 \cdots m$:

$$\mu_k[\lambda] = \frac{1}{2} \lambda^2 \Phi_b''' \hat{u}^2 \dot{v}_k + \frac{1}{6} \lambda^2 (\lambda - 3\lambda_b) \Phi_b'''' \hat{u}^3 \dot{v}_k$$

$$\mathcal{A}_{ijk} = \Phi_b''' \dot{v}_i \dot{v}_j \dot{v}_k$$

$$\mathcal{B}_{ijhk} = \Phi_b'''' \dot{v}_i \dot{v}_j \dot{v}_h \dot{v}_k - \Phi_b''(w_{ij} w_{hk} + w_{ih} w_{jk} + w_{ik} w_{jh}) \tag{2.8}$$

$$\mathcal{B}_{00ik} = \Phi_b'''' \hat{u}^2 \dot{v}_i \dot{v}_k - \Phi_b'' w_{00} w_{ik}$$

$$\mathcal{B}_{0ijk} = \Phi_b'''' \hat{u} \dot{v}_i \dot{v}_j \dot{v}_k$$

$$\mathcal{C}_{ik} = \Phi_b'' w_{00} w_{ik}$$

where the *implicit imperfection factors* μ_k are defined by the 4th order expansion of the unbalanced work on the fundamental path (i.e. $\mu_k[\lambda] := (\lambda\hat{p} - \Phi'[\lambda\hat{u}])\dot{v}_k$).

5. The equilibrium path is obtained by satisfying the projection of the equilibrium equation (2.1) onto $\mathcal{V}$. According to eqs, (2.7) and (2.8), we have

$$(\lambda_k - \lambda)\xi_k - \lambda_b(\lambda - \frac{\lambda_b}{2})\sum_{i=1}^{m}\xi_i\mathcal{C}_{ik} + \frac{1}{2}\sum_{i,j=1}^{m}\xi_i\xi_j\mathcal{A}_{ijk} + \frac{1}{2}(\lambda - \lambda_b)^2\sum_{i=1}^{m}\xi_i\mathcal{B}_{00ik}$$

$$+\frac{1}{2}(\lambda - \lambda_b)\sum_{i,j=1}^{m}\xi_i\xi_j\mathcal{B}_{0ijk} + \frac{1}{6}\sum_{i,j,h=1}^{m}\xi_i\xi_j\xi_h\mathcal{B}_{ijhk} + \mu_k[\lambda] = 0 \ , \quad k = 1\ldots m$$

(2.9)

Equation (2.9) corresponds to a highly nonlinear system in the $m+1$ unknowns $\lambda - \xi_i$ and can be solved using a standard path–following strategy. It provides the initial post–buckling behavior of the structure, including *modal interactions* and *jumping–after–bifurcation* phenomena.

Once the first analysis has been performed (step 1 to 4), the presence of small additional, load or displacement, imperfections can be taken into account in the postprocessing phase by adding additional coefficients to eq.(2.9), with a negligible computational extra–cost (see [**?**]). Further information about imperfection sensitivity analysis can be found in [**?**,**?**,**?**] and in the references therein.

2.2   Hellinger Reissner formulation

We know, from previous discussions, that a mixed interpolation can be really convenient in nonlinear analysis. Compatible interpolations actually mean a loss in our full freedom in tuning the interpolation, so they hardly provide the best choice. Consider however that the assumption of a mixed or a compatible interpolation does not necessarily imply the use of a mixed or compatible format in the problem description as it might seems by eqs. (**??**) and (**??**). In fact, the two formats only differ in the use of stress and displacement variables or of displacement variables alone. We can change from a mixed to a compatible format simply by expressing stress variables in terms of the displacement ones or, conversely, change from a compatible format to a mixed one by explicitly introducing the stress variables and their relations to the displacement ones.

To clarify this point, we can refer to the Hessian defined by eq.(**??**). By assuming an interpolation based on eqs. (**??**) and (**??**), it will be directly obtained as

$$\mathbf{K}_m[\boldsymbol{u}] := \sum_e \mathcal{A}_e \left(\begin{bmatrix} -\mathbf{H}_e & \mathbf{D}_e[\mathbf{d}_e] \\ \mathbf{D}_e^T[\mathbf{d}_e] & \mathbf{G}_e[\mathbf{d}_e,\, \mathbf{t}_e] \end{bmatrix} \right) \tag{2.10a}$$

where matrix $\mathbf{G}_e$ is defined by

$$\mathbf{G}_e[\mathbf{d}_e,\, \mathbf{t}_e] := \frac{\partial(\mathbf{D}_e^T \mathbf{t}_e)}{\partial \mathbf{d}_e} = \sum_k \left[\frac{\partial \mathbf{D}_k}{\partial \mathbf{d}_e} \right] t_k \tag{2.10b}$$

$\mathbf{D}_k$ and t_k being the k–th columns of matrix $\mathbf{D}_e$ and t_k the k–th component of vector $\mathbf{t}_e$ and summation being extended to all components of $\mathbf{t}_e$. That is, denoting with index G the assembled global matrices, we obtain a mixed format

$$\mathbf{K}_m[\boldsymbol{u}] := \begin{bmatrix} -\mathbf{H}_G & \mathbf{D}_G[\mathbf{d}_G] \\ \mathbf{D}_G^T[\mathbf{d}_G] & \mathbf{G}_G[\mathbf{d}_G,\, \mathbf{t}_G] \end{bmatrix} \tag{2.10c}$$

which, however, can be reduced to a compatible format by static condensation:

$$\mathbf{K}_c[\boldsymbol{u}] := \mathbf{D}_G^T[\mathbf{d}_G]\mathbf{H}_G^{-1}\mathbf{D}_G[\mathbf{d}_G] + \mathbf{G}_G[\mathbf{d}_G,\, \mathbf{t}_G]$$

Obviously, this rewriting does not change the element interpolation or its behavior, but only the *format* of its description..

Conversely, by introducing the compatibility assumption (**??**), the Hessian is obtained in compatible format

$$\mathbf{K}_c[\mathbf{u}] := \sum_e \mathcal{A}_e \left(\mathbf{K}_{0e}[\mathbf{d}_e] + \mathbf{G}_e[\mathbf{d}_e] \right)$$

matrix $\mathbf{K}_{0e}$ being defined by

$$\mathbf{K}_{0e}[\mathbf{d}_e] := \int_e \mathbf{B}_\varepsilon[s]^T \mathbf{H}[s]^{-1} \mathbf{B}_\varepsilon[s] \, d\boldsymbol{s} \tag{2.10d}$$

However, by an appropriate setting of matrices $\tilde{\mathbf{D}}_e$ and $\tilde{\mathbf{H}}_e$, the latter can be rewritten in the form

$$\mathbf{K}_{0e}[\mathbf{d}_e] = \tilde{\mathbf{D}}_e^T \tilde{\mathbf{H}}_e^{-1} \tilde{\mathbf{D}}_e$$

and so, by introducing the further equation

$$\tilde{\mathbf{t}}_e = \tilde{\mathbf{H}}_e^{-1} \tilde{\mathbf{D}}_e[\mathbf{d}_e]\mathbf{d}_e$$

it can be split into the same mixed format as eq.(2.10a). Also in this case, the rewriting does not change the element nature, but only the format of its description.

The mixed or compatible formats, while completely equivalent in principle, behave very differently when implemented either in path following or asymptotic solution strategies. This is an important, even if frequently misunderstood, point in practical computations which has been widely discussed in [**?**,**?**]. By referring readers to these papers and to the general discussion given in [**?**] for more details, we only recall here that both numerical strategies described in Section 2 need function $\boldsymbol{K}[\boldsymbol{u}]$ to be appropriately smooth in its controlling variables $\boldsymbol{u}$. In path–following analysis, its smoothness will imply having $\boldsymbol{K}[\boldsymbol{u}] \approx \tilde{\boldsymbol{K}} := \boldsymbol{K}[\boldsymbol{u}_0]$ when $\boldsymbol{u}$ moves in the neighborhood of $\boldsymbol{u}_0$ of interest, so allowing a fast convergence of the Newton iterative process. Analogously, matrix $\boldsymbol{K}[\boldsymbol{u}]$ being the Hessian of the strain energy, its smoothness implies, in asymptotic analysis, that the higher–order energy term neglected in the $4th$–order expansion (**??**) be really irrelevant, so allowing an accurate recovery of the equilibrium path. We know that the smoothness of a nonlinear function strictly depends on the choice of the set of its control variables, that is on the format of its description, and can change noticeably when referring to another, even corresponding, set. As a consequence, the mixed and compatible format, even if referring to the same problem, can be characterized by a different smoothness and so

they behave differently in practice, when used within a numerical solution process. Actually, the compatible format is particularly sensitive to what we call *extrapolation locking* in [**?**, **?**] which can produce a loss of convergence, when used in path–following analysis, or unacceptable errors in the path recovery, when used in asymptotic analysis. These inconveniences are easily avoided by changing to a mixed format.

2.3   On the use of 3D rotations

The nonlinear analysis of spatial structures depends on 3D rotations algebra. A great amount of work on this topic is available in the literature see [**?**, **?**, **?**, **?**, **?**]).

Finite 3D rotations can be directly represented in terms of an orthogonal tensor R that is a member of the nonlinear manifold SO(3). In coordinate representation, the rotation tensor R becomes a 3×3 orthogonal matrix that, by exploiting the orthogonality property $R^{-1} = R^{T}$, is a function of only three parameters. However it may not be convenient to express the configuration changes through variables belonging to a nonlinear manifold due to the complications involved in the successive variations (see [**?**]). A useful way to express R in terms of the quantities lying in a vector space is that of Rodrigues [**?**]:

$$R\left[\boldsymbol{\theta}\right] = I + \frac{\sin\theta}{\theta}W[\boldsymbol{\theta}] + \frac{(1-\cos\theta)}{\theta^{2}}W^{2}[\boldsymbol{\theta}] \qquad (2.11)$$

$$\boldsymbol{W}[\boldsymbol{\theta}] \equiv \text{spin}\,[\boldsymbol{\theta}] = \begin{bmatrix} 0 & -\theta_3 & \theta_2 \\ \theta_3 & 0 & -\theta_1 \\ -\theta_2 & \theta_1 & 0 \end{bmatrix} \tag{2.12}$$

which uses the rotation vectors $\boldsymbol{\theta} = [\theta_1, \theta_2, \theta_3]^T$, $\theta = \sqrt{\theta_1^2 + \theta_2^2 + \theta_3^2}$ being the magnitude of the rotation vector. This representation uses a minimal set of parameters, is singularity free and gives a one–to–one correspondence in the range $0 \leq \theta < 2\pi$ (see [**?**]). Making $\boldsymbol{R}_\theta \equiv \boldsymbol{R}[\boldsymbol{\theta}]$ and $\boldsymbol{W}_\theta \equiv \boldsymbol{W}[\boldsymbol{\theta}]$, equation (2.11) is equivalent to the exponential map

$$\boldsymbol{R}_\theta = \boldsymbol{I} + \boldsymbol{W}_\theta + \frac{\boldsymbol{W}_\theta^2}{2!} + \ldots = \sum_{n=0}^{\infty} \frac{\boldsymbol{W}_\theta^n}{n!} = \exp(\boldsymbol{W}_\theta) \tag{2.13}$$

The inverse relation is given by

$$\boldsymbol{\theta} = \frac{\arcsin \omega}{\omega} \boldsymbol{\omega} \tag{2.14a}$$

$\boldsymbol{\omega}$ being the axial vector of the skew–symmetric part of $\boldsymbol{R}_\theta$, implicitly defined by

$$\boldsymbol{W}[\boldsymbol{\omega}] = \frac{1}{2}(\boldsymbol{R}_\theta - \boldsymbol{R}_\theta^T) \tag{2.14b}$$

and ω the Euclidian norm of $\boldsymbol{\omega}$. By a Taylor expansion we obtain

$$\boldsymbol{\theta} = (1 + \frac{1}{6}\omega^2 + \frac{3}{40}\omega^4 + \ldots)\boldsymbol{\omega} \tag{2.14c}$$

The extraction of the rotation vector by the rotation matrix $\boldsymbol{R}_\theta$, as defined by eqs. (2.14), will from now on be denoted by $\boldsymbol{\theta} \equiv \log[\boldsymbol{R}_\theta]$.

The most commonly used approach in defining structural models involving 3D rotations is to express the kinematics in terms of the spin

variations δW which, as pointed out by Nour-Omid and Rankin [**?**], are the quantities associated through virtual works with the common accepted definition of moments. In this case, using eq. (2.13), the variation δR of R could be expressed in terms of the infinitesimal rotations defined by the spin δW:

$$\delta R = R \delta W \qquad\qquad (2.15)$$

If the current rotation R is known, eq. (2.15) allows for a simple expression of the first variations of the strain energy required by the equilibrium condition (2.1).

Remembering that R belongs to a nonlinear manifold, the successive variations of the energy quickly become increasingly complicated [**?**]. This does not however present a real problem in the path–following analysis, which requires the accurate evaluation of the first variations of energy with respect to the configuration variables and exploits the second variations only to define an iteration matrix to be used within a Newton–like scheme. Thus a rough evaluation of these variations, obtained through simplified formulas, can be sufficient for the analysis. The only difficulty in this context is related to the evaluation of the current rotation R, which requires a rather expensive multiplicative updating process. Consequently, a large amount of research has been devoted to setting up an efficient updating (see [**?**] for further details on this topic).

The use of the rotation vector θ to express 3D rotations, as intro-

duced in [**?**, **?**, **?**, **?**], allows the multiplicative updating to be avoided, but introduces an additional nonlinear relation through eq. (2.11). The main advantage is, however, the possibility of describing the configuration in terms of variables belonging to a linear manifold thereby allowing the strain energy variations to be evaluated accurately through standard directional derivatives. This is particularly useful within asymptotic analysis, where an accurate evaluation of these variations, up to fourth–order, is necessary. It becomes even more necessary when using the standard asymptotic formulation presented in section **??**, which requires that the configuration manifold $\mathcal{U}$ be linear. Accordingly, the rotation vector θ will be assumed as configuration variables in the sequel. It will also be shown that, rather simple general rules can be derived in order to obtain explicit expressions for the energy variations needed by the analysis.

Chapter 3

Corotational formulation

The goal of the corotational approach is to split the element motion into two parts: a rigid and a deformational one, thus providing an easy way to recover an objective structural modeling. The rigid part is defined, on average, as the motion of a corotational frame (CR observer) which translates and rotates with the element from the initial reference configuration to the current one. The deformational part is the local motion seen by the CR observer, within this frame. It can be made small enough with an appropriate mesh refinement, allowing the differences between pointwise and element average rotations to be reduced. Since the strains depend only on the deformational part, which can be assumed to be small, they can be described using simplified kinematical relationships: in particular, a linearized kinematics, as the simplest choice, or a more refined quadratic kinematics, for bet-

ter accuracy. The former choice allows standard linear finite elements to be reused as recognized by Rankin [?, ?]. The latter choice requires a nonlinear description of the element, while still allowing the usual simplifying "technical" assumptions for the element modeling, due to the assumption of small deformations.

Corotational description of motion has its origins in the polar decomposition theorem (see [?]). According to this theorem, the total deformation of a continuous body can be decomposed into a rigid body motion and a local deformation. In finite element implementations, this decomposition can be performed using a local CR frame that rotates and translates with each element (Gauss point). The advantage is that the nonlinearity of the problem is transferred to the coordinate transformation between the fixed and corotational systems, and the local displacements can be assumed small enough, in the CR frame, to allow strains to be obtained through linear or a simplified nonlinear strain–displacement relationships, without introducing significant errors. In fact, the strain energy thus obtained prove to be objective with respect to rigid body motions of the element and its accuracy can be increased as required with a mesh refinement. Furthermore, we can reuse linear finite element libraries [?, ?] thereby avoiding the need for objective interpolations [?, ?, ?] as occurs in other descriptions of the body motion. Conversely, the presence of rotation matrices, which lie in a nonlinear manifold and combine with a multiplicative rule, no-

ticeably complicates the algebra for obtaining exact expressions for the variations of the strain energy higher than the first order ones.

The corotational approach has been widely used as a basic tool for describing the configuration changes within the incremental–iterative path–following analysis [?, ?]. In this context, it requires explicit expressions for the first two variations of the strain energy. Only the first variation, used for checking the equilibrium, actually needs to be evaluated exactly. Even a rough estimate for the second one is generally sufficient, because it is only employed for defining a suitable iteration matrix to be used within a Newton–like solution process [?]. Consequently research in this area has been largely devoted to representing the first corotational derivative in an easy form, and to developing robust and computationally fast schemes for the iterative updating of the configuration.

By this choice, displacement interpolation can be set in the form

$$\bar{d}[s] = B_d[s] \, g[d_e] \qquad (3.1)$$

where vector $\bar{d}_e := g_e[d_e]$ is the representation of d_e in the corotational system and the vectorial function $g_e[\cdot]$ expresses the change in the observer rules defined by equations (20a) of [?]. We obtain a frame–invariant interpolation rule which, even being nonlinear, allows us to decouple the *internal* (element) derivation of functions $\varrho_e[\bar{d}_e]$ and $D_e[\bar{d}_e]$, referred to the corotational system, from the *external* (global)

corotational transformation ruled by $g_e[d_e]$. We need some algebra to obtain derivatives of the nonlinear function $g_e[d_e]$. These can, however, be obtained in standard recursive form and so are easily managed in FEM analysis, as shown in [**?**]. Furthermore, corotational displacements, ruled by $\bar{d}_e$, are only related to the distortion of the element and so, by mesh refinement, they can be made small enough to allow the use of the same interpolation laws derived from the linear analysis, without introducing noticeable interpolation locking. The smallness of $\bar{d}_e$ also allows an evaluation of the strain displacement relationships $\varrho[\bar{d}]$ through its Taylor expansion (see [**?**] for details) without any noticeable loss in accuracy. A 2nd–order expansion is usually adopted while a 1st–order can be sufficient with fine meshes. It is worth mentioning that when using a linear approximation, the element description will coincide, in the corotational framing, with that of linear theory, so allowing a direct reuse of standard software libraries already implemented for linear analysis. This is a great advantage, as pointed out by Rankin in the pioneering paper of 1988 [**?**]. In the sequel we will refer to this approach, which was also followed in [**?**] and [**?**], as *Standard Corotational*.

An alternative to the corotational interpolation, which can be used for the same purpose within path–following analysis, is provided by the so called *Updated Lagrangian* interpolation. Essentially, it is based on the use of an element fixed framing, which is, however, taken only

within a single incremental step of the analysis and is updated, once the step is accomplished, to fit the new alignment of the element. This approach is obviously simpler than the corotational one, because it does not need the computation of the derivatives of $\boldsymbol{g}_e[\boldsymbol{d}_e]$, and so it is frequently used in nonlinear analysis. Conversely, if it is coupled with a standard linear interpolation it requires very small incremental steps to avoid a loss in accuracy. Moreover, a certain care is required in the updating scheme to recover geometrical coherence, as much as possible, and to avoid that the error deriving from the use of a simplified strain/displacement relationship can accumulate in the incremental process. Actually, we have to be very careful, especially in the presence of coupled buckling, because losing even minor aspects of the nonlinear behavior can result in the mislaying of secondary bifurcations and modal jumping phenomena within the path recovery.

3.1   Strain energy in the CR frame

Let's assume a fixed frame with versors $\{\boldsymbol{e}_1, \boldsymbol{e}_2, \boldsymbol{e}_3\}$ and consider the motion described by the point displacement $\boldsymbol{d}[\boldsymbol{X}]$ and rotation $\boldsymbol{\varphi}[\boldsymbol{X}]$ vector fields, $\boldsymbol{X}$ being the position of the point in the reference configuration with respect to the fixed frame. The corotational versors are defined by

$$\boldsymbol{i}_k = \boldsymbol{Q}\boldsymbol{e}_k \quad \text{with} \quad \boldsymbol{Q} \equiv \boldsymbol{R}\left[\boldsymbol{\alpha}\right], \quad k = 1 \ldots 3. \tag{3.2}$$

where $\boldsymbol{\alpha}$ is the rigid rotation vector and $\boldsymbol{c}$ the translation vector which defines the CR motion. Using simple geometric considerations and omitting the dependence on $\boldsymbol{X}$, for an easy notation, the deformational local part of $\boldsymbol{d}[\boldsymbol{X}]$ can be described by the expressions

$$\boldsymbol{d}_c = \boldsymbol{Q}^T(\boldsymbol{X} + \boldsymbol{d} - \boldsymbol{c}) - \boldsymbol{X} \tag{3.3}$$

where $\boldsymbol{d}_c$ collects the components of the deformational displacement.

Similarly, the rotation vector of the local part of point rotation $\boldsymbol{R} := \boldsymbol{R}[\boldsymbol{\varphi}]$ is expressed by

$$\boldsymbol{\varphi}_c = \log(\boldsymbol{R}_c) \quad \text{with} \quad \boldsymbol{R}_c = \boldsymbol{Q}^T \boldsymbol{R}[\boldsymbol{\varphi}] \tag{3.4}$$

The point strain will be a function of the deformational displacement and rotation:

$$\boldsymbol{\varepsilon} = \boldsymbol{\varepsilon}[\boldsymbol{d}_c, \boldsymbol{\varphi}_c]$$

Assuming that $\boldsymbol{d}_c$ and $\boldsymbol{\varphi}_c$ are small, the constitutive laws can be taken as linear. Then, it is possible to express the finite element strain energy, in mixed form, as

$$\Phi_e[u] := \int_{\Omega_e} \left\{ \boldsymbol{\sigma} \cdot \boldsymbol{\varepsilon}[\boldsymbol{d}_c, \boldsymbol{\varphi}_c] - \frac{1}{2} \boldsymbol{\sigma} \cdot \boldsymbol{E}^{-1} \boldsymbol{\sigma} \right\} d\Omega_e \tag{3.5}$$

where $\boldsymbol{\sigma}$ is the stress associated with the elastic tensor $\boldsymbol{E}$ to the strain and Ω_e is the finite element domain. Exploiting the element interpolation laws, (3.5) can be rewritten, in discrete form, as:

$$\Phi_e[u] = \boldsymbol{\beta}_e^T \boldsymbol{\varrho}[\boldsymbol{d}_{ce}] - \frac{1}{2} \boldsymbol{\beta}_e^T \boldsymbol{H}_c \boldsymbol{\beta}_e \tag{3.6}$$

$\boldsymbol{\beta}_e$ being the vector of the element stress parameters and ϱ the associated vector of the strains, as a function of the displacement element vector $\boldsymbol{d}_{ce}$ collecting deformational displacements $\boldsymbol{d}_{ck}$ and rotations $\boldsymbol{\varphi}_{ck}$ of all k–th finite element nodes (or a relevant linear combination of them). Finally $\boldsymbol{K}_c^{-1}$ is the Clapeyron compliance matrix provided by the complementary energy equivalence

$$\frac{1}{2}\boldsymbol{\beta}_e^T \boldsymbol{H}_c \boldsymbol{\beta}_e = \frac{1}{2}\int_{\Omega_e} \boldsymbol{\sigma} \cdot \boldsymbol{E}^{-1}\boldsymbol{\sigma}\, d\Omega_e \quad , \quad \forall \quad \boldsymbol{\beta}_e,\, \boldsymbol{\sigma}[\boldsymbol{\beta}_e]$$

Exploiting the smallness of deformational displacements, we assume that ϱ can have, at most, the following quadratic expression in terms of $\boldsymbol{d}_{ce}$:

$$\varrho = \varrho_l[\boldsymbol{d}_{ce}] + \varrho_q[\boldsymbol{d}_{ce}, \boldsymbol{d}_{ce}] \tag{3.7}$$

where $\varrho_l[\boldsymbol{d}_{ce}] = \boldsymbol{D}\boldsymbol{d}_{ce}$ is a linear relationship while the j–th component of the symmetric bilinear quadratic part of ϱ_q is defined as:

$$\varrho_{qj}[\boldsymbol{d}_{ce}, \boldsymbol{d}_{ce}] = \frac{1}{2}\boldsymbol{d}_{ce}^T \boldsymbol{\Psi}_j \boldsymbol{d}_{ce} \quad , \quad \boldsymbol{\Psi}_j = \boldsymbol{\Psi}_j^T$$

with $j = 1\ldots n_\rho$, n_ρ being the dimension of vector ϱ.

The discrete expression of the strain energy (3.6) becomes

$$\Phi_e[u] = \boldsymbol{\beta}_e^T \boldsymbol{B}\boldsymbol{d}_{ce} + \frac{1}{2}\boldsymbol{d}_{ce}^T \boldsymbol{\Psi}[\boldsymbol{\beta}_e]\boldsymbol{d}_{ce} - \frac{1}{2}\boldsymbol{\beta}_e^T \boldsymbol{H}_c \boldsymbol{\beta}_e \tag{3.8a}$$

where $\boldsymbol{\Psi}[\boldsymbol{\beta}_e] = \sum_j \boldsymbol{\beta}_e \boldsymbol{\Psi}_j$. Using a linear strain measure ($\varrho_q \approx 0$), it reduces to the common expression of the linear elastic case

$$\Phi_e[u] = \boldsymbol{\beta}_e^T \boldsymbol{B}\boldsymbol{d}_{ce} - \frac{1}{2}\boldsymbol{\beta}_e^T \boldsymbol{H}_c \boldsymbol{\beta}_e \tag{3.8b}$$

3.1.1 A remark on the corotational description

Letting $\boldsymbol{\alpha}_e$ be the CR rotation vector associated to the average rigid rotation of the element and

$$\boldsymbol{Q}_e = \boldsymbol{R}[\boldsymbol{\alpha}_e] \tag{3.9}$$

the CR formulation is based on two fundamental steps:

a) the definition of kinematical relationships (3.3) and (3.4) that express a purely *geometric nonlinear relation*

$$\boldsymbol{d}_{ce} = \boldsymbol{d}_{0e} + \boldsymbol{d}_g[\boldsymbol{\alpha}_e, \, \boldsymbol{d}_e] \tag{3.10}$$

between the element displacement vector in the CR ($\boldsymbol{d}_{ce}$) and fixed frames ($\boldsymbol{d}_e$). We assume that $\boldsymbol{d}_g[\boldsymbol{\alpha}_e, \, \boldsymbol{0}] = \boldsymbol{0}$, so that $\boldsymbol{d}_{0e}$ will be the initial deformational displacement vector for $\boldsymbol{d}_e = \boldsymbol{0}$. The additive rule in (3.10) is possible thanks to the assumption that both $\boldsymbol{d}_{0e}$ and $\boldsymbol{d}_g$ are small.

b) a *local modeling* of the mechanical behavior of the structures, which is an implicitly defined expression of the strain energy of the element in terms of local CR finite element parameters, which is written in the simplified form (3.8), because of the assumption of small local displacements.

Note that the geometrical nonlinearities are essentially contained in eq. (3.10), while the local modeling only implies standard finite element

procedures and, if using expression (3.8b), corresponds to a linear FEM modeling. The corotational approach then leads to an efficient way of reusing standard FEM technology in a nonlinear context.

3.2 Strain energy in the fixed frame

The CR rotation vector $\boldsymbol{\alpha}_e$ will be a function of the current displacement vector $\boldsymbol{d}_e$:

$$\boldsymbol{\alpha}_e := \boldsymbol{\alpha}_e[\boldsymbol{d}_e] \qquad (3.11)$$

The explicit expression of this function will depend on the particular element which is used and is based on the best compromise between algebraic simplicity and accuracy, the latter being essentially related to the smallness of the deformational part of the motion. By substituting eq. (3.11) into (3.10), we can express $\boldsymbol{d}_{ce}$ as a function of $\boldsymbol{d}_e$ alone:

$$\boldsymbol{d}_{ce} = \boldsymbol{d}_{0e} + \boldsymbol{g}[\boldsymbol{d}_e] \qquad (3.12)$$

The combination of eqs. (3.8) and (3.10) allows the element energy to be expressed in terms of the element vector

$$\boldsymbol{u}_e := \{\boldsymbol{\beta}_e, \, \boldsymbol{d}_e\}^T \qquad (3.13)$$

which collects all parameters defining the element configuration in a single vector and can be related to the global vector $\boldsymbol{u}$, expressing the overall configuration of the assemblage, through the known relation

$$\boldsymbol{u}_e = \boldsymbol{A}_e \boldsymbol{u} \qquad (3.14)$$

where matrix $\boldsymbol{A}_e$ implicitly contains the link constraints between elements. This allows the energy to be expressed as an algebraic nonlinear function of $\boldsymbol{u}$:

$$\Phi[u] := \sum_e \Phi_e[u]$$

The asymptotic approach requires the evaluation of the 2nd, 3rd and 4th variations of the energy by correspondence to a configuration which can be either the initial u_0 or the bifurcation one u_b. In both cases, through an appropriate configuration updating process, we refer to a configuration characterized by $\boldsymbol{d}_e = \boldsymbol{0}$, the initial stresses and (small) deformational displacements being described by the element vectors $\boldsymbol{\beta}_{0e}$ and $\boldsymbol{d}_{0e}$.

To express the strain energy variations, it is convenient to refer to the fourth order Taylor expansion of $\boldsymbol{g}[d_e]$ starting from a configuration characterized by $\boldsymbol{d}_e = \boldsymbol{0}$:

$$\boldsymbol{g}[\boldsymbol{d}_e] = \boldsymbol{g}_1[\boldsymbol{d}_e] + \frac{1}{2}\boldsymbol{g}_2[\boldsymbol{d}_e, \boldsymbol{d}_e] + \frac{1}{6}\boldsymbol{g}_3[\boldsymbol{d}_e, \boldsymbol{d}_e, \boldsymbol{d}_e] + \frac{1}{24}\boldsymbol{g}_4[\boldsymbol{d}_e, \boldsymbol{d}_e, \boldsymbol{d}_e, \boldsymbol{d}_e] + \cdots \quad (3.15)$$

where $\boldsymbol{g}_n$, $n = 1 \cdots 4$ are n–multilinear symmetric forms which express the nth Frechèt variations of function $\boldsymbol{g}[\boldsymbol{d}_e]$.

The relevant strain energy variations are reported here, for the simpler case of *linear local modeling* defined by eq. (3.8b), and then extended to the *quadratic local modeling* defined by eq. (3.8a).

We will denote with u_i ($i = 1 \ldots 4$) a generic variation of the configuration field u, with $\boldsymbol{u}_i$ the corresponding global configuration vector in

the FEM discretization and with $\boldsymbol{u}_{ie} = \boldsymbol{A}_e \boldsymbol{u}_i$ the finite element configuration vector collecting both displacement and stress element vectors: $\boldsymbol{u}_{ie} = \{\boldsymbol{\beta}_{ie}, \boldsymbol{d}_{ie}\}^T$. With the same notation $\boldsymbol{u}_0$ and $\boldsymbol{u}_{0e}$ are the global and element reference configuration vectors.

3.2.1 Second variations using linear local modeling

Second energy variations are used in the evaluation of the fundamental mode $\hat{u}$ (through eq. (2.3)) and of the bifurcation modes $\dot{v}_i$ (through eq. (2.4)). In both cases, using expansion (3.15) and the energy expression (3.8a), the contribution of the element to the energy variation can be expressed as

$$\Phi_e^{''} u_1 u_2 = \boldsymbol{\beta}_{1e}^T \boldsymbol{\varrho}_1[\boldsymbol{d}_{2e}] + \boldsymbol{\beta}_{2e}^T \boldsymbol{\varrho}_1[\boldsymbol{d}_{2e}] - \boldsymbol{\beta}_{1e}^T \boldsymbol{H}_e \boldsymbol{\beta}_{2e} + \boldsymbol{\beta}_{0e}^T \boldsymbol{\varrho}_2[\boldsymbol{d}_{1e}, \boldsymbol{d}_{2e}] \quad \text{(3.16a)}$$

where $\boldsymbol{\varrho}_1$ and $\boldsymbol{\varrho}_2$ are defined by

$$\boldsymbol{\varrho}_1[\boldsymbol{d}_{je}] = \boldsymbol{B}_e \boldsymbol{g}_1[\boldsymbol{d}_{je}] \qquad \boldsymbol{\varrho}_2[\boldsymbol{d}_{1e}, \boldsymbol{d}_{2e}] = \boldsymbol{B}_e \boldsymbol{g}_2[\boldsymbol{d}_{1e}, \boldsymbol{d}_{2e}] \qquad j = 1, 2 \quad \text{(3.16b)}$$

and then the constant matrix that depend only from the linear element $\boldsymbol{B}_e = \int_{\Omega e} \boldsymbol{P}^T \boldsymbol{D} \boldsymbol{U} d\Omega_e$ and $\boldsymbol{H}_e = \int_{\Omega e} \boldsymbol{P}^T \boldsymbol{E}^{-1} \boldsymbol{P} d\Omega_e$ we can rewrite the second energy variation as element independent:

$$\Phi_e^{''} u_1 u_2 = \boldsymbol{\beta}_{1e}^T \boldsymbol{B}_e \boldsymbol{g}_1[\boldsymbol{d}_{2e}] + \boldsymbol{\beta}_{2e}^T \boldsymbol{B}_e \boldsymbol{g}_1[\boldsymbol{d}_{2e}] - \boldsymbol{\beta}_{1e}^T \boldsymbol{H}_e \boldsymbol{\beta}_{2e} + \boldsymbol{\beta}_{0e}^T \boldsymbol{B}_e \boldsymbol{g}_2[\boldsymbol{d}_{1e}, \boldsymbol{d}_{2e}]$$

in order to form the hessian of the above quantity eq. (3.16) can be rearranged in a more convenient compact form using the follows energy

equivalences:

$$\boldsymbol{\beta}_{0e}^T \boldsymbol{B}_e \boldsymbol{g}_2[\boldsymbol{d}_{1e}, \boldsymbol{d}_{2e}] = \boldsymbol{d}_{1e}^T \boldsymbol{G}_e[\boldsymbol{r}_{0e}]\boldsymbol{d}_{2e}$$

where $\boldsymbol{r}_{0e} = \boldsymbol{\beta}_{0e}^T \boldsymbol{B}_e$. Then the matrix $\boldsymbol{G}_e[r_{0e}]$ became very simple and fast to compute.

Introducing also the matrices $\boldsymbol{L}_1$

$$\boldsymbol{g}_s[\boldsymbol{d}_{je}] = \boldsymbol{L}_1 \boldsymbol{d}_{je} \qquad (j = 1 \ldots s) \tag{3.17}$$

in wich s is the variation order.

For the corresponding vector format of the secondary energy variation can be expressed in the following format

$$\delta \boldsymbol{u}^T \boldsymbol{S}[\boldsymbol{u}_1] = \Phi^{''} u_1 \delta u \tag{3.18}$$

$$\Phi_e^{''} u_1 \delta u = \delta u^T \boldsymbol{S}_e[\boldsymbol{u}_{1e}] \quad , \quad \boldsymbol{S}_e = \begin{bmatrix} -\boldsymbol{H}_e \boldsymbol{\beta}_{1e} + \boldsymbol{B}_e \boldsymbol{L}_1 \boldsymbol{d}_{1e} \\ \boldsymbol{L}_1^T \boldsymbol{B}_e^T \boldsymbol{\beta}_{2e} + \boldsymbol{G}_e[\boldsymbol{r}_{0e}]\boldsymbol{d}_{2e} \end{bmatrix} \tag{3.19}$$

and the corresponding matrix

$$\Phi_e^{''} u_1 u_2 = \boldsymbol{u}_{1e}^T \boldsymbol{K}_e \boldsymbol{u}_{2e} \quad , \quad \boldsymbol{K}_e = \begin{bmatrix} -\boldsymbol{H}_e & \boldsymbol{B}_e \boldsymbol{L}_1 \\ \boldsymbol{L}_1^T \boldsymbol{B}_e^T & \boldsymbol{G}_e[\boldsymbol{r}_{0e}] \end{bmatrix} \tag{3.20}$$

The mixed tangent matrix of the element $\boldsymbol{K}_e$ can be directly used, through a standard assemblage process, to obtain the overall Hessian matrix $\boldsymbol{K}$:

$$\Phi^{''} u_1 u_2 = \boldsymbol{u}_1^T \boldsymbol{K} \boldsymbol{u}_2 \quad , \quad \boldsymbol{H} := \sum_e \boldsymbol{A}_e^T \boldsymbol{K}_e \boldsymbol{A}_e \tag{3.21}$$

in wich the transfering operator from local reference configuration to the global one is:

$$\boldsymbol{A}_e = \begin{bmatrix} \boldsymbol{I} & \boldsymbol{0} \\ \boldsymbol{0} & \boldsymbol{E}_0^d \end{bmatrix}, \qquad \boldsymbol{E}_0^d = diag(\boldsymbol{E}_0) \tag{3.22}$$

allowing eqs. (2.3) and (2.4) to be rewritten in matrix form. In the previous eq. 3.22 the $\boldsymbol{E}_0^d$ collect in diagonal form n times $\boldsymbol{E}_0$ that rotates both displacement and rotations for each node in the element and $\boldsymbol{I}$ have the same dimension of the $\boldsymbol{\beta}$ vector. Numerically this procedure can be performed in a fast way operating block-wise trough the matrices.

3.2.2 Third variations using linear modeling

Third energy variations are used in eq. (2.8) for evaluating the third–order coefficients $\mathcal{A}_{ijk}$ and the third–order terms of the factors μ_k, which are scalar quantities obtained as variations with respect to known fields $\hat{u}$ and $\dot{v}_i$. They are also used in eq. (2.7) for evaluating the right–side of the equation which implicitly defines the quadratic modes w_{ij}. In this case we have to evaluate secondary force vector $\boldsymbol{s}[\boldsymbol{u}_1, \boldsymbol{u}_2]$ defined by the equivalence

$$\delta \boldsymbol{u}^T \boldsymbol{s}[\boldsymbol{u}_1, \boldsymbol{u}_2] = \Phi''' u_1 u_2 \delta u \tag{3.23}$$

δu being a generic virtual variation and $\delta \boldsymbol{u}$ its corresponding discrete representation. The element contribution to the scalar expressions is

easily evaluated using the general formula

$$\Phi_e''' u_1 u_2 u_3 = \boldsymbol{\beta}_{1e}^T \boldsymbol{\varrho}_2[\boldsymbol{d}_{2e}, \boldsymbol{d}_{3e}] + \boldsymbol{\beta}_{2e}^T \boldsymbol{\varrho}_2[\boldsymbol{d}_{3e}, \boldsymbol{d}_{1e}] + \boldsymbol{\beta}_{3e}^T \boldsymbol{\varrho}_2[\boldsymbol{d}_{1e}, \boldsymbol{d}_{2e}] \tag{3.24a}$$

$$+ \boldsymbol{\beta}_{0e}^T \boldsymbol{\varrho}_3[\boldsymbol{d}_{1e}, \boldsymbol{d}_{2e}, \boldsymbol{d}_{3e}]$$

where $\boldsymbol{\varrho}_2[\cdot, \cdot]$ is defined by (3.16b) and $\boldsymbol{\varrho}_3[\cdots]$ is obtained by

$$\boldsymbol{\varrho}_3[\boldsymbol{d}_{1e}, \boldsymbol{d}_{2e}, \boldsymbol{d}_{3e}] = \boldsymbol{B}_e \boldsymbol{g}_3[\boldsymbol{d}_{1e}, \boldsymbol{d}_{2e}, \boldsymbol{d}_{3e}] \tag{3.24b}$$

$$\boldsymbol{\beta}_{0e}^T \boldsymbol{\varrho}_3[\boldsymbol{d}_{1e}, \boldsymbol{d}_{2e}, \boldsymbol{d}_{3e}] = \boldsymbol{d}_{3e}^T \boldsymbol{G}_{e2}[\boldsymbol{r}_{0e}, \boldsymbol{d}_{1e}]\boldsymbol{d}_{2e} \tag{3.24c}$$

$$\Phi_e''' u_1 u_2 u_3 = \boldsymbol{\beta}_{1e}^T \boldsymbol{B}_e \boldsymbol{g}_2[\boldsymbol{d}_{2e}, \boldsymbol{d}_{3e}] + \boldsymbol{\beta}_{2e}^T \boldsymbol{B}_e \boldsymbol{g}_2[\boldsymbol{d}_{3e}, \boldsymbol{d}_{1e}] + \boldsymbol{\beta}_{3e}^T \boldsymbol{B}_e \boldsymbol{g}_2[\boldsymbol{d}_{1e}, \boldsymbol{d}_{2e}]$$

$$+ \boldsymbol{\beta}_{0e}^T \boldsymbol{B}_e \boldsymbol{g}_3[\boldsymbol{d}_{1e}, \boldsymbol{d}_{2e}, \boldsymbol{d}_{3e}]$$

$$\tag{3.24d}$$

When the vectorial expression (3.18) is needed, making $u_3 = \delta u$, eq. (3.24a) can be rearranged in the form

$$\Phi_e''' u_1 u_2 \delta u := \delta \boldsymbol{u}_e^T \boldsymbol{s}_e = \begin{bmatrix} \delta \boldsymbol{\beta}_e \\ \delta \boldsymbol{d}_e \end{bmatrix}^T \begin{bmatrix} \boldsymbol{s}_{et} \\ \boldsymbol{s}_{ed} \end{bmatrix} \tag{3.25}$$

where $\boldsymbol{s}_{et}$ and $\boldsymbol{s}_{ed}$ vectors may be obtained by using already defined operators:

$$\boldsymbol{s}_{et} = \boldsymbol{B}_e \boldsymbol{g}_2[\boldsymbol{d}_{1e}, \boldsymbol{d}_{2e}]$$

$$\tag{3.26}$$

$$\boldsymbol{s}_{ed} = (\boldsymbol{G}_e[\boldsymbol{r}_{1e}] + \boldsymbol{G}_{e2}[\boldsymbol{r}_{0e}, \boldsymbol{d}_{1e}])\boldsymbol{d}_{2e} + \boldsymbol{G}_e[\boldsymbol{r}_{2e}]\boldsymbol{d}_{1e}$$

The overall structural vector $\boldsymbol{s}$ is then obtained by a standard assemblage

$$\boldsymbol{s}[\boldsymbol{u}_1, \boldsymbol{u}_2] = \sum_e \boldsymbol{A}_e^T \boldsymbol{s}_e[\boldsymbol{u}_{1e}, \boldsymbol{u}_{2e}]$$

3.2.3   Fourth variations using linear local modeling

Fourth energy variations are used in eq. (2.8) for evaluating the fourth–order coefficients $\mathcal{B}_{ijhk}$ and the fourth–order terms in μ_k. The following general formula for the element contributions can be used.

$$
\begin{aligned}
\Phi_e^{''''} u_1 u_2 u_3 u_4 &= \boldsymbol{\beta}_{1e}^T \boldsymbol{\varrho}_3[\boldsymbol{d}_{2e}, \boldsymbol{d}_{3e}, \boldsymbol{d}_{4e}] + \boldsymbol{\beta}_{2e}^T \boldsymbol{\varrho}_3[\boldsymbol{d}_{3e}, \boldsymbol{d}_{4e}, \boldsymbol{d}_{1e}] \\
&\quad + \boldsymbol{\beta}_{3e}^T \boldsymbol{\varrho}_3[\boldsymbol{d}_{4e}, \boldsymbol{d}_{1e}, \boldsymbol{d}_{2e}] + \boldsymbol{\beta}_{4e}^T \boldsymbol{\varrho}_3[\boldsymbol{d}_{1e}, \boldsymbol{d}_{2e}, \boldsymbol{d}_{3e}] \\
&\quad + \boldsymbol{\beta}_{0e}^T \boldsymbol{\varrho}_4[\boldsymbol{d}_{1e}, \boldsymbol{d}_{2e}, \boldsymbol{d}_{3e}, \boldsymbol{d}_{4e}]
\end{aligned}
\tag{3.27}
$$

where function $\boldsymbol{\varrho}_4[\cdot]$ is obtained by

$$
\boldsymbol{\varrho}_4[\boldsymbol{d}_{1e}, \boldsymbol{d}_{2e}, \boldsymbol{d}_{3e}, \boldsymbol{d}_{4e}] = \boldsymbol{B}_e \boldsymbol{g}_4[\boldsymbol{d}_{1e}, \boldsymbol{d}_{2e}, \boldsymbol{d}_{3e}, \boldsymbol{d}_{4e}].
$$

3.3   Corotational scalar variations

Using (3.16b) and (3.24b) we can calculate the variations independently to the particular element but only by (3.15) in a power-full and general way. Using (3.4) and (3.3) the generic vector $\boldsymbol{g}[\boldsymbol{d}_e]$ can be expressed as:

$$
\boldsymbol{g}[\boldsymbol{d}_e] = \begin{bmatrix} \boldsymbol{g}^{(1)}[\boldsymbol{d}_e] \\ \vdots \\ \boldsymbol{g}^{(k)}[\boldsymbol{d}_e] \end{bmatrix}, \quad \boldsymbol{g}^{(k)}[\boldsymbol{d}_e] = \begin{bmatrix} \boldsymbol{d}_c^{(k)} \\ \boldsymbol{\varphi}_c^{(k)} \end{bmatrix}, \quad k = 1 \cdots N
\tag{3.28}
$$

in which N is the number of the nodes in the element.

3.3.1 Nodal variations

The variations can be performed node-by-node independently of the element formulation. For the first variation at the nodal parameter we have:

$$g_1^{(k)}[d_{e1}] = \begin{bmatrix} d_{c1}^{(k)}[d_{e1}] \\ \varphi_{c1}^{(k)}[d_{e1}] \end{bmatrix} \tag{3.29}$$

$$g_2^{(k)}[d_{e1}, d_{e2}] = \begin{bmatrix} d_{c2}^{(k)}[d_{e1}, d_{e2}] \\ \varphi_{c2}^{(k)}[\varphi_{e1}, \varphi_{e2}] \end{bmatrix} \tag{3.30}$$

$$g_3^{(k)}[d_{e1}, d_{e2}, d_{e3}] = \begin{bmatrix} d_{c3}^{(k)}[d_{e1}, d_{e2}, d_{e3}] \\ \varphi_{c3}^{(k)}[\varphi_{e1}, \varphi_{e2}, \varphi_{e3}] \end{bmatrix} \tag{3.31}$$

$$g_4^{(k)}[d_{e1}, d_{e2}, d_{e3}, d_{e4}] = \begin{bmatrix} d_{c4}^{(k)}[d_{e1}, d_{e2}, d_{e3}, d_{e4}] \\ \varphi_{c4}^{(k)}[\varphi_{e1}, \varphi_{e2}, \varphi_{e3}, \varphi_{e4}] \end{bmatrix} \tag{3.32}$$

Starting from (3.3) we can get the variations respect to $Q_1[d_e]$ and to d_{e1} evaluated at the point $d_e = 0$. The variations of a rotation matrix will be described after the following section within the variations being $R[\varphi_c]$ and $Q[d_e]$ both of the same format.

$$d_{c1}^{(k)} = d_{e1}^{(k)} - Q_1[d_{e1}]X^{(k)} \tag{3.33}$$

$$d_{c2}^{(k)} = Q_2[d_{e1}, d_{e2}]X^{(k)} - Q_1[d_{e1}]d_{e2}^{(k)} - Q_1[d_{e2}]d_{e1}^{(k)} \tag{3.34}$$

$$\boldsymbol{d}_{c3}^{(k)} = \boldsymbol{Q}_3[\boldsymbol{d}_{e1}, \boldsymbol{d}_{e2}, \boldsymbol{d}_{e3}]\boldsymbol{X}^{(k)} - \boldsymbol{Q}_2[\boldsymbol{d}_{e1}, \boldsymbol{d}_{e2}]\boldsymbol{d}_{e3}^{(k)}$$
$$- \boldsymbol{Q}_2[\boldsymbol{d}_{e2}, \boldsymbol{d}_{e3}]\boldsymbol{d}_{e1}^{(k)} - \boldsymbol{Q}_2[\boldsymbol{d}_{e3}, \boldsymbol{d}_{e1}]\boldsymbol{d}_{e2}^{(k)} \tag{3.35}$$

$$\boldsymbol{d}_{c4}^{(k)} = \boldsymbol{Q}_4[\boldsymbol{d}_{e1}, \boldsymbol{d}_{e2}, \boldsymbol{d}_{e3}, \boldsymbol{d}_{e4}]\boldsymbol{X}^{(k)}$$
$$- \boldsymbol{Q}_3[\boldsymbol{d}_{e1}, \boldsymbol{d}_{e2}, \boldsymbol{d}_{e3}]\boldsymbol{d}_{e4}^{(k)} - \boldsymbol{Q}_3[\boldsymbol{d}_{e2}, \boldsymbol{d}_{e3}, \boldsymbol{d}_{e4}]\boldsymbol{d}_{e1}^{(k)} \tag{3.36}$$
$$- \boldsymbol{Q}_3[\boldsymbol{d}_{e3}, \boldsymbol{d}_{e4}, \boldsymbol{d}_{e1}]\boldsymbol{d}_{e2}^{(k)} - \boldsymbol{Q}_3[\boldsymbol{d}_{e4}, \boldsymbol{d}_{e1}, \boldsymbol{d}_{e2}]\boldsymbol{d}_{e3}^{(k)}$$

As well as, we can get the variations of (3.4) respect to $\boldsymbol{w}_1^{(k)}[\boldsymbol{d}_{e1}]$ as defined in (**??**) $\boldsymbol{\varphi}_c^{(k)}[\boldsymbol{d}_e] = (1 + \frac{1}{6}w^2)\boldsymbol{w}[\boldsymbol{d}_e]$

$$\boldsymbol{\varphi}_{c1}^{(k)} = \boldsymbol{w}_1^{(k)}[\boldsymbol{d}_{e1}] \tag{3.37}$$

$$\boldsymbol{\varphi}_{c2}^{(k)} = \boldsymbol{w}_2^{(k)}[\boldsymbol{d}_{e1}, \boldsymbol{d}_{e2}] \tag{3.38}$$

$$\boldsymbol{\varphi}_{c3}^{(k)} = \boldsymbol{w}_3^{(k)}[\boldsymbol{d}_{e1}, \boldsymbol{d}_{e2}, \boldsymbol{d}_{e3}]$$
$$+ w_2^{(k)}[\boldsymbol{d}_{e1}, \boldsymbol{d}_{e2}] \, \boldsymbol{w}_1^{(k)}[\boldsymbol{d}_{e3}]$$
$$+ w_2^{(k)}[\boldsymbol{d}_{e2}, \boldsymbol{d}_{e3}] \, \boldsymbol{w}_1^{(k)}[\boldsymbol{d}_{e1}] \tag{3.39}$$
$$+ w_2^{(k)}[\boldsymbol{d}_{e3}, \boldsymbol{d}_{e1}] \, \boldsymbol{w}_1^{(k)}[\boldsymbol{d}_{e2}]$$

$$\boldsymbol{\varphi}_{c4}^{(k)} = \boldsymbol{w}_4^{(k)}[\boldsymbol{d}_{e1}, \boldsymbol{d}_{e2}, \boldsymbol{d}_{e3}, \boldsymbol{d}_{e4}]$$
$$+ w_2^{(k)}[\boldsymbol{d}_{e1}, \boldsymbol{d}_{e2}] \, \boldsymbol{w}_2^{(k)}[\boldsymbol{d}_{e3}, \boldsymbol{d}_{e4}] + w_2^{(k)}[\boldsymbol{d}_{e2}, \boldsymbol{d}_{e3}] \, \boldsymbol{w}_2^{(k)}[\boldsymbol{d}_{e4}, \boldsymbol{d}_{e1}]$$
$$+ w_2^{(k)}[\boldsymbol{d}_{e3}, \boldsymbol{d}_{e4}] \, \boldsymbol{w}_2^{(k)}[\boldsymbol{d}_{e1}, \boldsymbol{d}_{e2}] + w_2^{(k)}[\boldsymbol{d}_{e4}, \boldsymbol{d}_{e1}] \, \boldsymbol{w}_2^{(k)}[\boldsymbol{d}_{e2}, \boldsymbol{d}_{e3}] \tag{3.40}$$
$$+ w_2^{(k)}[\boldsymbol{d}_{e1}, \boldsymbol{d}_{e3}] \, \boldsymbol{w}_2^{(k)}[\boldsymbol{d}_{e4}, \boldsymbol{d}_{e2}] + w_2^{(k)}[\boldsymbol{d}_{e1}, \boldsymbol{d}_{e4}] \, \boldsymbol{w}_2^{(k)}[\boldsymbol{d}_{e2}, \boldsymbol{d}_{e3}]$$

In which the scalar w_2 is the second variation of $\frac{1}{6}\boldsymbol{w}^T\boldsymbol{w}$ in the equation **??** that for symmetry may be simplified as follows (omitting k for clearness):

$$
\begin{aligned}
w_2[\boldsymbol{d}_{e1}, \boldsymbol{d}_{e2}] &= (\boldsymbol{\varphi}_{c1}[\boldsymbol{d}_{e1}]^T \boldsymbol{\varphi}_{c1}[\boldsymbol{d}_{e2}] + \boldsymbol{\varphi}_{c1}[\boldsymbol{d}_{e2}]^T \boldsymbol{\varphi}_{c1}[\boldsymbol{d}_{e1}])/6 \\
&= (\boldsymbol{\varphi}_{c1}[\boldsymbol{d}_{e1}]^T \boldsymbol{\varphi}_{c1}[\boldsymbol{d}_{e2}])/3
\end{aligned}
\tag{3.41}
$$

Now will be performed the variation of

$$
\boldsymbol{w} = (\boldsymbol{Q}^T\boldsymbol{R} - \boldsymbol{Q}\boldsymbol{R}^T)/2,
$$

with respect the variables $\boldsymbol{Q}$ and $\boldsymbol{R}$ letting

$$
skew(\boldsymbol{T}) := (\boldsymbol{T} - \boldsymbol{T}^T)/2 \quad \text{and} \quad \boldsymbol{Q}_1^T = -\boldsymbol{Q}_1
$$

$$
\begin{aligned}
\boldsymbol{w}_1^{(k)}[\boldsymbol{d}_{e1}] &= skew(-\boldsymbol{Q}_1[\boldsymbol{d}_{e1}] + \boldsymbol{R}_1[\boldsymbol{\varphi}_{e1}^{(k)}]) \\
&= -\boldsymbol{Q}_1[\boldsymbol{d}_{e1}] + \boldsymbol{R}_1[\boldsymbol{\varphi}_{e1}^{(k)}]
\end{aligned}
\tag{3.42}
$$

$$
\boldsymbol{w}_2^{(k)}[\boldsymbol{d}_{e1}, \boldsymbol{d}_{e2}] = skew(-\boldsymbol{Q}_1[\boldsymbol{d}_{e1}]\boldsymbol{R}_1[\boldsymbol{\varphi}_{e2}^{(k)}] - \boldsymbol{Q}_1[\boldsymbol{d}_{e2}]\boldsymbol{R}_1[\boldsymbol{\varphi}_{e1}^{(k)}])
\tag{3.43}
$$

$$
\begin{aligned}
\boldsymbol{w}_3^{(k)}[\boldsymbol{d}_{e1}, \boldsymbol{d}_{e2}, \boldsymbol{d}_{e3}] = skew(&\boldsymbol{R}_3[\boldsymbol{\varphi}_{e1}^{(k)}, \boldsymbol{\varphi}_{e2}^{(k)}, \boldsymbol{\varphi}_{e3}^{(k)}] - \boldsymbol{Q}_3[\boldsymbol{d}_{e1}, \boldsymbol{d}_{e2}, \boldsymbol{d}_{e3}] \\
&+ \boldsymbol{Q}_2[\boldsymbol{d}_{e1}, \boldsymbol{d}_{e2}]\boldsymbol{R}_1[\boldsymbol{\varphi}_{e3}^{(k)}] - \boldsymbol{Q}_1[\boldsymbol{d}_{e1}]\boldsymbol{R}_2[\boldsymbol{\varphi}_{e2}^{(k)}, \boldsymbol{\varphi}_{e3}^{(k)}] \\
&+ \boldsymbol{Q}_2[\boldsymbol{d}_{e2}, \boldsymbol{d}_{e3}]\boldsymbol{R}_1[\boldsymbol{\varphi}_{e1}^{(k)}] - \boldsymbol{Q}_1[\boldsymbol{d}_{e2}]\boldsymbol{R}_2[\boldsymbol{\varphi}_{e3}^{(k)}, \boldsymbol{\varphi}_{e1}^{(k)}] \\
&+ \boldsymbol{Q}_2[\boldsymbol{d}_{e3}, \boldsymbol{d}_{e1}]\boldsymbol{R}_1[\boldsymbol{\varphi}_{e2}^{(k)}] - \boldsymbol{Q}_1[\boldsymbol{d}_{e3}]\boldsymbol{R}_2[\boldsymbol{\varphi}_{e1}^{(k)}, \boldsymbol{\varphi}_{e2}^{(k)}])
\end{aligned}
\tag{3.44}
$$

$$\boldsymbol{w}_4^{(k)}[\boldsymbol{d}_{e1}, \boldsymbol{d}_{e2}, \boldsymbol{d}_{e3}, \boldsymbol{d}_{e4}] = skew(\boldsymbol{Q}_2[\boldsymbol{d}_{e1}, \boldsymbol{d}_{e3}]\boldsymbol{R}_2[\boldsymbol{\varphi}_{e4}^{(k)}, \boldsymbol{\varphi}_{e2}^{(k)}] + \boldsymbol{Q}_2[\boldsymbol{d}_{e2}, \boldsymbol{d}_{e4}]\boldsymbol{R}_2[\boldsymbol{\varphi}_{e1}^{(k)}, \boldsymbol{\varphi}_{e3}^{(k)}]$$

$$+ \boldsymbol{Q}_2[\boldsymbol{d}_{e1}, \boldsymbol{d}_{e1}]\boldsymbol{R}_2[\boldsymbol{\varphi}_{e3}^{(k)}, \boldsymbol{\varphi}_{e4}^{(k)}] + \boldsymbol{Q}_2[\boldsymbol{d}_{e2}, \boldsymbol{d}_{e3}]\boldsymbol{R}_2[\boldsymbol{\varphi}_{e4}^{(k)}, \boldsymbol{\varphi}_{e1}^{(k)}]$$

$$+ \boldsymbol{Q}_2[\boldsymbol{d}_{e3}, \boldsymbol{d}_{e4}]\boldsymbol{R}_2[\boldsymbol{\varphi}_{e1}^{(k)}, \boldsymbol{\varphi}_{e2}^{(k)}] + \boldsymbol{Q}_2[\boldsymbol{d}_{e4}, \boldsymbol{d}_{e1}]\boldsymbol{R}_2[\boldsymbol{\varphi}_{e2}^{(k)}, \boldsymbol{\varphi}_{e3}^{(k)}]$$

$$- \boldsymbol{Q}_3[\boldsymbol{d}_{e1}, \boldsymbol{d}_{e2}, \boldsymbol{d}_{e3}]\boldsymbol{R}_1[\boldsymbol{\varphi}_{e4}^{(k)}] - \boldsymbol{Q}_3[\boldsymbol{d}_{e2}, \boldsymbol{d}_{e3}, \boldsymbol{d}_{e4}]\boldsymbol{R}_1[\boldsymbol{\varphi}_{e1}^{(k)}]$$

$$- \boldsymbol{Q}_3[\boldsymbol{d}_{e3}, \boldsymbol{d}_{e4}, \boldsymbol{d}_{e1}]\boldsymbol{R}_1[\boldsymbol{\varphi}_{e2}^{(k)}] - \boldsymbol{Q}_3[\boldsymbol{d}_{e4}, \boldsymbol{d}_{e1}, \boldsymbol{d}_{e2}]\boldsymbol{R}_1[\boldsymbol{\varphi}_{e3}^{(k)}]$$

$$- \boldsymbol{Q}_1[\boldsymbol{d}_{e1}]\boldsymbol{R}_3[\boldsymbol{\varphi}_{e4}^{(k)}, \boldsymbol{\varphi}_{e2}^{(k)}, \boldsymbol{\varphi}_{e3}^{(k)}] - \boldsymbol{Q}_1[\boldsymbol{d}_{e2}]\boldsymbol{R}_3[\boldsymbol{\varphi}_{e1}^{(k)}, \boldsymbol{\varphi}_{e3}^{(k)}, \boldsymbol{\varphi}_{e4}^{(k)}]$$

$$- \boldsymbol{Q}_1[\boldsymbol{d}_{e3}]\boldsymbol{R}_3[\boldsymbol{\varphi}_{e2}^{(k)}, \boldsymbol{\varphi}_{e4}^{(k)}, \boldsymbol{\varphi}_{e1}^{(k)}] - \boldsymbol{Q}_1[\boldsymbol{d}_{e4}]\boldsymbol{R}_3[\boldsymbol{\varphi}_{e3}^{(k)}, \boldsymbol{\varphi}_{e1}^{(k)}, \boldsymbol{\varphi}_{e2}^{(k)}])$$

$$(3.45)$$

Variations of the nodal rotation $\boldsymbol{R}[\boldsymbol{\varphi}_e^{(k)}]$ matrices and of corotational frame $\boldsymbol{Q}$ must be performed in order to get all complete variations scheme:

$$\boldsymbol{Q}_2[\boldsymbol{d}_{e1}, \boldsymbol{d}_{e2}] = (\quad \boldsymbol{Q}_1[\boldsymbol{d}_{e1}]\boldsymbol{Q}_1[\boldsymbol{d}_{e2}]$$
$$+ \boldsymbol{Q}_1[\boldsymbol{d}_{e2}]\boldsymbol{Q}_1[\boldsymbol{d}_{e1}])/2 \tag{3.46a}$$

$$\boldsymbol{Q}_3[\boldsymbol{d}_{e1}, \boldsymbol{d}_{e2}, \boldsymbol{d}_{e3}] = (\quad \boldsymbol{Q}_1[\boldsymbol{d}_{e1}]\boldsymbol{Q}_2[\boldsymbol{d}_{e2}, \boldsymbol{d}_{e3}]$$
$$+ \boldsymbol{Q}_1[\boldsymbol{d}_{e2}]\boldsymbol{Q}_2[\boldsymbol{d}_{e3}, \boldsymbol{d}_{e1}] \tag{3.46b}$$
$$+ \boldsymbol{Q}_1[\boldsymbol{d}_{e3}]\boldsymbol{Q}_2[\boldsymbol{d}_{e1}, \boldsymbol{d}_{e2}])/3$$

$$\boldsymbol{Q}_4[\boldsymbol{d}_{e1}, \boldsymbol{d}_{e2}, \boldsymbol{d}_{e3}, \boldsymbol{d}_{e4}] = (\quad \boldsymbol{Q}_1[\boldsymbol{d}_{e1}]\boldsymbol{Q}_3[\boldsymbol{d}_{e2}, \boldsymbol{d}_{e3}, \boldsymbol{d}_{e4}]$$
$$+ \boldsymbol{Q}_1[\boldsymbol{d}_{e2}]\boldsymbol{Q}_3[\boldsymbol{d}_{e3}, \boldsymbol{d}_{e4}, \boldsymbol{d}_{e1}]$$
$$+ \boldsymbol{Q}_1[\boldsymbol{d}_{e3}]\boldsymbol{Q}_3[\boldsymbol{d}_{e4}, \boldsymbol{d}_{e1}, \boldsymbol{d}_{e2}] \tag{3.46c}$$
$$+ \boldsymbol{Q}_1[\boldsymbol{d}_{e4}]\boldsymbol{Q}_3[\boldsymbol{d}_{e1}, \boldsymbol{d}_{e2}, \boldsymbol{d}_{e3}])/4$$

and for completeness we will report also variations of nodal rotation matrices, however it have the same format of 3.46:

$$\boldsymbol{R}_1[\boldsymbol{\varphi}_{e1}^{(k)}] = spin(\boldsymbol{\varphi}_{c1}^{(k)}) \tag{3.47a}$$

$$\boldsymbol{R}_2[\boldsymbol{\varphi}_{e1}^{(k)}, \boldsymbol{\varphi}_{e2}^{(k)}] = (\quad \boldsymbol{R}_1[\boldsymbol{\varphi}_{e1}^{(k)}]\boldsymbol{R}_1[\boldsymbol{\varphi}_{e2}^{(k)}]$$
$$+ \boldsymbol{R}_1[\boldsymbol{\varphi}_{e2}^{(k)}]\boldsymbol{R}_1[\boldsymbol{\varphi}_{e1}^{(k)}] \,)/2 \tag{3.47b}$$

$$\boldsymbol{R}_3[\boldsymbol{\varphi}_{e1}^{(k)}, \boldsymbol{\varphi}_{e2}^{(k)}, \boldsymbol{\varphi}_{e3}^{(k)}] = (\quad \boldsymbol{R}_1[\boldsymbol{\varphi}_{e1}^{(k)}]\boldsymbol{R}_2[\boldsymbol{\varphi}_{e2}^{(k)}, \boldsymbol{\varphi}_{e3}^{(k)}]$$
$$+ \boldsymbol{R}_1[\boldsymbol{\varphi}_{e2}^{(k)}]\boldsymbol{R}_2[\boldsymbol{\varphi}_{e3}^{(k)}, \boldsymbol{\varphi}_{e1}^{(k)}] \tag{3.47c}$$
$$+ \boldsymbol{R}_1[\boldsymbol{\varphi}_{e3}^{(k)}]\boldsymbol{R}_2[\boldsymbol{\varphi}_{e1}^{(k)}, \boldsymbol{\varphi}_{e2}^{(k)}] \,)/3$$

$$\boldsymbol{R}_4[\boldsymbol{\varphi}_{e1}^{(k)}, \boldsymbol{\varphi}_{e2}^{(k)}, \boldsymbol{\varphi}_{e3}^{(k)}, \boldsymbol{\varphi}_{e4}^{(k)}] = (\quad \boldsymbol{R}_1[\boldsymbol{\varphi}_{e1}^{(k)}]\boldsymbol{R}_3[\boldsymbol{\varphi}_{e2}^{(k)}, \boldsymbol{\varphi}_{e3}^{(k)}, \boldsymbol{\varphi}_{e4}^{(k)}]$$
$$+ \boldsymbol{R}_1[\boldsymbol{\varphi}_{e2}^{(k)}]\boldsymbol{R}_3[\boldsymbol{\varphi}_{e3}^{(k)}, \boldsymbol{\varphi}_{e4}^{(k)}, \boldsymbol{\varphi}_{e1}^{(k)}]$$
$$+ \boldsymbol{R}_1[\boldsymbol{\varphi}_{e3}^{(k)}]\boldsymbol{R}_3[\boldsymbol{\varphi}_{e4}^{(k)}, \boldsymbol{\varphi}_{e1}^{(k)}, \boldsymbol{\varphi}_{e2}^{(k)}] \tag{3.47d}$$
$$+ \boldsymbol{R}_1[\boldsymbol{\varphi}_{e4}^{(k)}]\boldsymbol{R}_3[\boldsymbol{\varphi}_{e1}^{(k)}, \boldsymbol{\varphi}_{e2}^{(k)}, \boldsymbol{\varphi}_{e3}^{(k)}] \,)/4$$

To be noted that it is omitted only the first variation of $\boldsymbol{Q}$ that depend on the particular chose of the corotational element frame and also its first variation. The first variation of the corotational reference will be given with the particular element used.

All the others variations can be obtained then in a powerful way by using the chain–rule derivation. Obviously, an optimized implementation of these routines need to be performed in order to make performavit the algorithm.

3.4   Concluding remarks

As we can see in all of 3.46, 3.47, **??**, **??** the dependence on element formulation it is only on the definition of $\boldsymbol{Q}[\boldsymbol{d}_e]$ and its first variation. Then, this scheme may be used for to derive the corotational variations for any finite element within a framework whit $6\ DOF$ for node independently of the number of nodes and of the particular linear finite element.

To be noted that the methods it is very powerful because only we need to define first variation of $\boldsymbol{Q}$ for each new element that need to be implemented. In fact, all successive variations are *recursively* dependent from these of previous order. This strong characteristic provide a fully way to generalize the corotational Koiter's method to all kind of linear finite element already know.

Chapter 4

Linear Flat shell model

4.1 Introduction

Consider a plate referred to a Cartesian coordinate frame (O, x, y, z), with the origin O on the mid-surface Ω and the z-axis in the thickness direction, $-h/2 \leq z \leq h/2$, where h is the plate thickness. Let $\partial\Omega$ be the boundary of Ω. The first-order shear deformable theory, often called Reissner-Mindlin theory, and Plane Stress theory are employed. Thus it is assumed that

$$u(x, y, z) = u(x, y) + z\theta_y(x, y)$$
$$v(x, y, z) = v(x, y) - z\theta_x(x, y) \qquad (4.1)$$
$$w(x, y, z) = w(x, y)$$

where u, v, w are the displacements along the x, y and z axes, respectively, and θ_x, θ_y are the rotations of the transverse normal about the x

and y axes. The sign convention is depicted in Figure **??**.

By refer to the plane $z = 0$ the compatibility equations can be written as follows

$$\boldsymbol{\epsilon} = \boldsymbol{D}_m \boldsymbol{u}, \quad \boldsymbol{\chi} = \boldsymbol{D}_b \boldsymbol{\theta}, \quad \boldsymbol{\gamma} = \boldsymbol{D}_s w + \boldsymbol{\theta}, \tag{4.2}$$

where vectors $\boldsymbol{u}$, $\boldsymbol{\theta}$, $\boldsymbol{\chi}$ and $\boldsymbol{\gamma}$ collect, respectively, the rotations, the curvatures and the shear strains,

$$\boldsymbol{u} = \begin{bmatrix} u \\ v \end{bmatrix}, \quad \boldsymbol{\epsilon} = \begin{bmatrix} \epsilon_x \\ \epsilon_y \\ \epsilon_{xy} \end{bmatrix}, \quad \boldsymbol{\theta} = \begin{bmatrix} \theta_x \\ \theta_y \end{bmatrix}, \quad \boldsymbol{\chi} = \begin{bmatrix} \chi_x \\ \chi_y \\ \chi_{xy} \end{bmatrix}, \quad \boldsymbol{\gamma} = \begin{bmatrix} \gamma_x \\ \gamma_y \end{bmatrix},$$

$$\tag{4.3}$$

and operators $\boldsymbol{D}_m$, $\boldsymbol{D}_b$ (see **[?]** about changing on sign) and $\boldsymbol{D}_s$ are given by

$$\mathbf{D}_m = \begin{bmatrix} \partial/\partial x & 0 \\ 0 & \partial/\partial y \\ \partial/\partial y & \partial/\partial x \end{bmatrix}, \quad \mathbf{D}_b = \begin{bmatrix} 0 & \partial/\partial y \\ \partial/\partial x & 0 \\ \partial/\partial x & \partial/\partial y \end{bmatrix}, \quad \mathbf{D}_s = \begin{bmatrix} \partial/\partial x \\ \partial/\partial y \end{bmatrix}.$$

$$\tag{4.4}$$

The equilibrium equations can be obtained *via* the principle of virtual work in the form

$$\boldsymbol{D}_m^* \boldsymbol{N} = \boldsymbol{n}, \quad \boldsymbol{D}_b^* \boldsymbol{M} + \boldsymbol{S} = \boldsymbol{m}, \quad \boldsymbol{D}_s^* \boldsymbol{S} = q, \tag{4.5}$$

where vectors N, M and S collect, respectively, the membrane, the

moment and shear resultants,

$$\boldsymbol{N} = \begin{bmatrix} N_x \\ N_y \\ N_{xy} \end{bmatrix}, \quad \mathbf{M} = \begin{bmatrix} M_x \\ M_y \\ M_{xy} \end{bmatrix}, \quad \mathbf{S} = \begin{bmatrix} S_x \\ S_y \end{bmatrix}, \quad (4.6)$$

q and **m**, **n** are the prescribed loads in Ω and $\mathbf{D}^*$ adjoint to $\mathbf{D}$:

$$\mathbf{D}^* = \mathbf{D}^{\mathrm{T}}. \quad (4.7)$$

For a linearly elastic material, the constitutive equations can be written as

$$\mathbf{N} = \mathbf{C}_m \boldsymbol{\epsilon}, \quad \mathbf{M} = \mathbf{C}_b \chi, \quad \mathbf{S} = \mathbf{C}_s \gamma, \quad (4.8)$$

where $\mathbf{C}_m$, $\mathbf{C}_b$ and $\mathbf{C}_s$ are the matrices of membrane, bending and transverse shear moduli. In the isotropic case, the elasticity matrices specialize as:

$$\boldsymbol{C}_m = \frac{Eh}{(1-\nu^2)} \begin{bmatrix} 1 & \nu & 0 \\ \nu & 1 & 0 \\ 0 & 0 & \frac{(1-\nu)}{2} \end{bmatrix}, \quad \begin{aligned} \boldsymbol{C}_b &= \frac{h^2}{12}\boldsymbol{C}_m, \\ \\ \boldsymbol{C}_s &= kGh\boldsymbol{I}_2 \end{aligned} \quad (4.9)$$

being E the Young's modulus, G the shear modulus, ν the Poisson's ratio and k a correction factor to account for non-uniform distribution of shear stresses through the thickness. The equilibrium problem of linear elastic shear deformable shell is ruled by Equations (4.2), (4.5) and (4.8) in Ω, together with appropriate boundary conditions on $\partial\Omega$.

The variational formulation is based on a Hellinger-Reissner functional:

$$\Phi[u] = \int_\Omega \left(\boldsymbol{\sigma}^T \boldsymbol{\varepsilon}[u] - \frac{1}{2} \boldsymbol{\sigma}^T \boldsymbol{E}^{-1} \boldsymbol{\sigma} \right) \mathrm{d}\Omega - \Phi_{\text{ext}} \tag{4.10}$$

where

$$\boldsymbol{\sigma} = \begin{bmatrix} \boldsymbol{N} \\ \boldsymbol{M} \\ \boldsymbol{S} \end{bmatrix}, \quad \boldsymbol{E} = \begin{bmatrix} \boldsymbol{E}_m & 0 & 0 \\ 0 & \boldsymbol{E}_b & 0 \\ 0 & 0 & \boldsymbol{E}_s \end{bmatrix}, \quad \boldsymbol{\varepsilon} = \begin{bmatrix} \boldsymbol{\epsilon} \\ \boldsymbol{\chi} \\ \boldsymbol{\gamma} \end{bmatrix} \tag{4.11}$$

.

The variational formulation of the problem described in terms of stress resultants and generalized displacements is

$$\Phi[u] = -\frac{1}{2} \int_\Omega \left(\mathbf{N}^T \mathbf{E}_m^{-1} \mathbf{N} + \mathbf{M}^T \mathbf{E}_b^{-1} \mathbf{M} + \mathbf{S}^T \mathbf{E}_s^{-1} \mathbf{S} \right) \mathrm{d}\Omega +$$
$$\int_\Omega \left[\mathbf{N}^T \mathbf{D}_m \mathbf{u} + \mathbf{M}^T \mathbf{D}_b \theta + \mathbf{S}^T (\mathbf{D}_s w + \boldsymbol{\theta} \right] \mathrm{d}\Omega - \Phi_{\text{ext}}, \tag{4.12}$$

where Π_{ext} is the work done by external (body and boundary) loads.

4.2 Isoparametric formulation

The element geometry is represented based on a 4-node scheme. A general quadrilateral element is considered in a local Cartesian system of coordinates (see Figure **??**). The transformation between the local coordinates x and y and the natural coordinates ξ and η is given by

$$\begin{bmatrix} x \\ y \end{bmatrix} = \begin{bmatrix} a_1\xi + a_2\eta + a_3\xi\eta \\ b_1\xi + b_2\eta + b_3\xi\eta \end{bmatrix}, \tag{4.13}$$

where

$$
\begin{bmatrix} a_1 & b_1 \\ a_2 & b_2 \\ a_3 & b_3 \end{bmatrix} = \frac{1}{4} \begin{bmatrix} -1 & 1 & 1 & -1 \\ 1 & -1 & 1 & -1 \\ -1 & -1 & 1 & 1 \end{bmatrix} \begin{bmatrix} x_1 & y_1 \\ x_2 & y_2 \\ x_3 & y_3 \\ x_4 & y_4 \end{bmatrix},
\tag{4.14}
$$

being x_i and y_i the local coordinates of the i-th corner node. The Jacobian **J** of the coordinate transformation defined by Equation (4.13) can be written as

$$
\mathbf{J} = \mathbf{J}_0 + \mathbf{J}_1,
\tag{4.15}
$$

$$
\mathbf{J}_0 = \begin{bmatrix} a_1 & b_1 \\ a_3 & b_3 \end{bmatrix}, \quad \mathbf{J}_1 = \begin{bmatrix} a_2\eta & b_2\eta \\ a_2\xi & b_2\xi \end{bmatrix},
$$

and its determinant j is

$$
j = \det \mathbf{J} = j_0 + j_1\xi + j_2\eta,
\tag{4.16}
$$

$$
j_0 = a_1 b_3 - a_3 b_1, \quad j_1 = a_1 b_2 - a_2 b_1, \quad j_2 = a_2 b_3 - a_3 b_2.
$$

For later convenience, the following quantities are introduced:

$$
\bar{\xi} = \xi + \frac{j_2}{j_0}\xi\eta, \quad \bar{\eta} = \eta + \frac{j_1}{j_0}\xi\eta.
\tag{4.17}
$$

It can be easily verified that quantities $\bar{\xi}$, $\bar{\eta}$ are linearly related to the local coordinates x, y through the Jacobian of the mapping (4.13) eval-

uated at the origin ($\xi = \eta = 0$):

$$
\begin{bmatrix} x \\ y \end{bmatrix} = \mathbf{J}_0^{\mathrm{T}} \begin{bmatrix} \bar{\xi} \\ \bar{\eta} \end{bmatrix}.
\tag{4.18}
$$

Thus, for a general quadrilateral element, $\bar{\xi}$ and $\bar{\eta}$ define a skew coordinate system, as shown in Figure **??**.

4.3   Assumed displacement

In order to avoid locking a linked interpolation was used in both case of in–plane ad out–of–plane displacements interpolation. All four edges of the quadrilater may be treated as 2-D beam element with shear deformation:

$$
\boldsymbol{n}_{ij} = \begin{bmatrix} \cos\alpha_{ij} \\ \sin\alpha_{ij} \end{bmatrix} = \frac{1}{l_{ij}} \begin{bmatrix} \Delta_y \\ \Delta_x \end{bmatrix}
\tag{4.19}
$$

$$
\boldsymbol{t}_{ij} = \begin{bmatrix} -\sin\alpha_{ij} \\ \cos\alpha_{ij} \end{bmatrix} = \frac{1}{l_{ij}} \begin{bmatrix} -\Delta_x \\ \Delta_y \end{bmatrix}
\tag{4.20}
$$

$$
l_{ij} = \sqrt{\Delta_x^2 + \Delta_y^2}
\tag{4.21}
$$

.

The general interpolation function for any typical edge can be expressed [30, 31] by:

$$u(\xi, \eta) = \sum_{i=1}^{4} U_i u_i + \sum_{i=1}^{4} \frac{\Delta y_i}{8} L_i^*(\theta_{zj} - \theta_{zi})$$

$$v(\xi, \eta) = \sum_{i=1}^{4} U_i v_i - \sum_{i=1}^{4} \frac{\Delta x_i}{8} L_i^*(\theta_{zj} - \theta_{zi})$$

$$w(\xi, \eta) = \sum_{i=1}^{4} U_i w_i - \sum_{i=1}^{4} \frac{\Delta y_i}{8} L_i^*(\theta_{xj} - \theta_{xi}) + \sum_{i=1}^{4} \frac{\Delta x_i}{8} L_i^*(\theta_{yj} - \theta_{yi})$$

$$\theta_x(\xi, \eta) = \sum_{i=1}^{4} U_i \theta_{xi}$$

$$\theta_y(\xi, \eta) = \sum_{i=1}^{4} U_i \theta_{yi}$$

$$\theta_z(\xi, \eta) = \sum_{i=1}^{4} U_i \theta_{zi}$$

(4.22)

where

$$U_i = \frac{1}{4}(1 + \xi_i \xi)(1 + \eta_i \eta); \ i = 1, .., 4 \tag{4.23}$$

$$L_i = \begin{cases} \frac{1}{2}(1 - \xi^2)(1 + \eta_i \eta); & i = 1, 3 \\ \frac{1}{2}(1 - \eta^2)(1 + \xi_i \xi); & i = 2, 4 \end{cases} \tag{4.24}$$

and

$$j = \begin{cases} i + 1 & i = 1, 2, 3 \\ 1 & i = 4 \end{cases}$$

In the above set of equation ξ and eta are the element natural coordinates and ξ_i and η_i are the value of ξ and η at node i.

Note that the drilling degrees of freedom (θ_{zi}) are not true nodal rotation but are referred to as "rotational connectors" Almann and enter the finite element approximation as differences in rotational connectors.

This element with drilling degree of freedom rotation have 24 degrees of freedom.

The displacement field may be expressed in a matrix format as follows:

$$\boldsymbol{u} = \boldsymbol{U}_u \boldsymbol{q}_u + \boldsymbol{L} \boldsymbol{q}_{dr}, \quad \boldsymbol{\theta} = \boldsymbol{U}_\theta \boldsymbol{q}_\theta, \quad w = \boldsymbol{U}_w \boldsymbol{q}_w + \boldsymbol{L} \boldsymbol{q}_\theta \tag{4.25}$$

4.4 Assumed stresses

The stress field can be chose in different way. For example as proposed in the Chapter "Shell" of [**?**].

Different assumptions may be considered for bending and membrane stress. In particular were used an isostatic hybrid formulation for bending part by following [32] and a suitable membrane stress by following [**?**].

4.4.1 Assumed stresses for bending

In this section, a strategy to select the stress approximation in a rational way is presented. Stresses are approximated independently on

each element and should satisfy the equilibrium equations pointwise within each element.

It is well recognized that for desirable element properties suitable local coordinates should be used to express the stresses. In particular, Yuan et al. [**?**] showed that stress approximations for membrane elements can be made to satisfy a priori the equilibrium equations by employing the skew coordinates $\bar{\xi}$, $\bar{\eta}$. According to this and excluding, at the moment, the presence of external body forces, the generalized stresses are initially assumed as an uncoupled polynomial expansion in terms of $\bar{\xi}$, $\bar{\eta}$, depending on 18 parameters:

$$
\left[\begin{array}{c} \mathbf{M} \\ \mathbf{S} \end{array}\right] = \left[\begin{array}{ccc|cc} \tilde{\mathbf{P}}_b & \mathbf{0} & \mathbf{0} & \mathbf{0} & \mathbf{0} \\ \mathbf{0} & \tilde{\mathbf{P}}_b & \mathbf{0} & \mathbf{0} & \mathbf{0} \\ \mathbf{0} & \mathbf{0} & \tilde{\mathbf{P}}_b & \mathbf{0} & \mathbf{0} \\ \hline \mathbf{0} & \mathbf{0} & \mathbf{0} & \tilde{\mathbf{P}}_s & \mathbf{0} \\ \mathbf{0} & \mathbf{0} & \mathbf{0} & \mathbf{0} & \tilde{\mathbf{P}}_s \end{array}\right] \left[\begin{array}{c} \beta_b \\ \beta_s \end{array}\right], \tag{4.26}
$$

where β_b and β_s are the parameters, local to each element, governing bending and shear modes, respectively, and

$$
\tilde{\mathbf{P}}_b = \left[\begin{array}{cccc} 1 & \bar{\xi} & \bar{\eta} & \bar{\xi}\bar{\eta} \end{array}\right], \quad \tilde{\mathbf{P}}_s = \left[\begin{array}{ccc} 1 & \bar{\xi} & \bar{\eta} \end{array}\right]. \tag{4.27}
$$

Notice that the initially assumed approximation for bending moments, $\tilde{\mathbf{P}}_b$, is complete up to the bi-linear term. This term is introduced aiming at equilibrating the linear shear terms.

The next step is to constrain the initially assumed stresses, Equation (4.26), in order to satisfy the equilibrium equations. This can be achieved (in the absence of body forces) by enforcing the following condition on each individual element Ω_e:

$$\int_{\Omega_e} \begin{bmatrix} \theta \\ w \end{bmatrix}^{\mathrm{T}} \begin{bmatrix} \mathbf{D}_b^* & \hat{\mathbf{I}}^{\mathrm{T}} \\ \mathbf{0} & \mathbf{D}_s^* \end{bmatrix} \begin{bmatrix} \mathbf{M} \\ \mathbf{S} \end{bmatrix} \mathrm{d}\Omega = 0 \qquad \forall \theta, w. \qquad (4.28)$$

Indeed, it is sufficient to require that the above condition is met for the assumed displacement approximation. Then, substituting Equations (**??**) and (4.26) into Equation (4.28) and making the resultant condition satisfied for all $\mathbf{q}_\theta$ and $\mathbf{q}_w$, a set of algebraic equations is obtained, which is used to reduce the number of independent stress parameters. This results in the following coupled approximation

$$\begin{bmatrix} \mathbf{M} \\ \mathbf{S} \end{bmatrix} = \left[\begin{array}{cccccc|cc} 1 & 0 & 0 & a_1^2\bar\eta & a_3^2\bar\xi & -a_1\bar\xi - a_3\bar\eta & 0 \\ 0 & 1 & 0 & b_1^2\bar\eta & b_3^2\bar\xi & 0 & -b_1\bar\xi - b_3\bar\eta \\ 0 & 0 & 1 & a_1 b_1\bar\eta & a_3 b_3\bar\xi & 0 & 0 \\ \hline 0 & 0 & 0 & 0 & 0 & 1 & 0 \\ 0 & 0 & 0 & 0 & 0 & 0 & 1 \end{array} \right.$$

$$\left. \begin{array}{cc|cc} -a_1^2\bar\xi\bar\eta & -a_3^2\bar\xi\bar\eta & 0 & 0 \\ -b_1^2\bar\xi\bar\eta & -b_3^2\bar\xi\bar\eta & 0 & 0 \\ -a_1 b_1\bar\xi\bar\eta & -a_3 b_3\bar\xi\bar\eta & a_3\bar\xi + a_1\bar\eta & b_3\bar\xi + b_1\bar\eta \\ \hline a_1\bar\eta & a_3\bar\xi & \dfrac{a_3^2 - a_1^2}{a_1 b_3 - b_1 a_3} & \dfrac{b_3 a_3 - b_1 a_1}{a_1 b_3 - b_1 a_3} \\ b_1\bar\eta & b_3\bar\xi & \dfrac{b_1 a_1 - b_3 a_3}{a_1 b_3 - b_1 a_3} & \dfrac{b_1^2 - b_3^2}{a_1 b_3 - b_1 a_3} \end{array} \right] \begin{bmatrix} \beta_b \\ \beta_s \end{bmatrix} \qquad (4.29)$$

ruled by 11 β-parameters. It can be shown that the above approximation satisfies the equilibrium equations in the homogeneous form pointwise. Moreover it has been checked that the stress approximation (4.29), together with the linked interpolation (**??**), leads to a finite element with correct rank (i.e., with no spurious kinematic modes), which is locking-free and passes all the patch tests. Notice that for regular element geometry Equation (4.29) reduces to the LH4 approximation proposed by Spilker and Munir in [**?**].

A number of suitable functions can be adopted to represent the incompatible displacements and derive stress approximations with the desired properties. All these approximations are good candidates for successful plate elements. In the present work, the final stress approximation is obtained by simply selecting the first nine stress modes in Equation (4.29). In this way, the number of stress parameters is reduced to the minimum without introducing zero energy modes. Moreover, it can be immediately realized that the above stress approximation guarantees, in regular geometry, the capability to model beam-like problems, with linearly varying moment and constant shear ("cylindrical bending"). For further convenience, the resultant stress approximation is put in the compact form

$$
\begin{bmatrix} \mathbf{M} \\ \mathbf{S} \end{bmatrix} = \begin{bmatrix} \mathbf{P}_b & \mathbf{P}_{bs} \\ \mathbf{0} & \mathbf{P}_s \end{bmatrix} \begin{bmatrix} \beta_b \\ \beta_s \end{bmatrix}.
\tag{4.30}
$$

To take into account for the presence of body forces, the original hybrid stress model is followed [**?**]: a particular solution of the equilibrium equations is added to Equation (4.30). The resulting expression reads as

$$
\begin{bmatrix} \mathbf{M} \\ \mathbf{S} \end{bmatrix} = \begin{bmatrix} \mathbf{P}_b & \mathbf{P}_{bs} \\ \mathbf{0} & \mathbf{P}_s \end{bmatrix} \begin{bmatrix} \beta_b \\ \beta_s \end{bmatrix} + \begin{bmatrix} \mathbf{M}_p \\ \mathbf{S}_p \end{bmatrix}, \tag{4.31}
$$

where $\mathbf{M}_p$ and $\mathbf{S}_p$ are known functions which satisfy Equation (4.5) in Ω_e. In the case of uniform loading $q = const$ and $\mathbf{m}^{\mathrm{T}} = \begin{bmatrix} m_x & m_y \end{bmatrix} = const$, they can be chosen as

$$
\mathbf{M}_p = \begin{bmatrix} \frac{1}{4}qx^2 + m_x x \\ \frac{1}{4}qy^2 - m_y y \\ 0 \end{bmatrix}, \quad \mathbf{S}_p = -\frac{1}{2}q \begin{bmatrix} x \\ y \end{bmatrix}. \tag{4.32}
$$

This expression is adopted for the numerical tests presented in Section 5.

4.4.2 Assumed stresses for membrane

In order to obtain a shell element ruled by a minimal set of parameters, due to use of drilling rotations, we need 9 tension parameters. Then the follow interpoaltion was been used for the membrane tensions:

$$
[\boldsymbol{N}] = \begin{bmatrix} 1 & 0 & 0 & \xi & 0 & \eta & 0 & \eta^2 & 0 \\ 0 & 1 & 0 & 0 & \xi & 0 & \eta & 0 & \xi^2 \\ 0 & 0 & 1 & -\eta & 0 & 0 & -\xi & 0 & 0 \end{bmatrix} [\boldsymbol{\beta}_m] = [\boldsymbol{P}_m][\boldsymbol{\beta}_m] \tag{4.33}
$$

that in [**?**] was showed are free of locking and exploits good performance in usual cases of membrane problems.

4.5   Finite element equations

Here, basing on the hybrid stress formulation and the assumptions made in the previous section, the finite element equations are derived.

Introducing the assumed displacements (**??**) and stresses (4.31) into the hybrid stress functional (**??**) referred to the single element the following discrete element equations is obtained:

Then, the equation 4.12 may be recast in a discrete form by using the finite element formulation above descripted and the final numerical form become:

$$\Phi[u] = \boldsymbol{\beta}^T \boldsymbol{B} \boldsymbol{q} - \frac{1}{2} \boldsymbol{\beta}^T \boldsymbol{H} \boldsymbol{\beta} \tag{4.34}$$

in which:

$$\boldsymbol{H} = \begin{bmatrix} \boldsymbol{H}_s^s + \boldsymbol{H}_s^b & \boldsymbol{H}_{bs}^b & \boldsymbol{0} \\ \left(\boldsymbol{H}_{bs}^b\right)^T & \boldsymbol{H}_b^b & \boldsymbol{0} \\ \boldsymbol{0} & \boldsymbol{0} & \boldsymbol{H}_m^m \end{bmatrix}, \; \boldsymbol{B} = \begin{bmatrix} \boldsymbol{B}_s^w & \boldsymbol{B}_{bs}^\theta + \boldsymbol{B}_s^{w\theta} + \boldsymbol{B}_s^\theta & \boldsymbol{0} & \boldsymbol{0} \\ \boldsymbol{0} & \boldsymbol{B}_b^\theta & \boldsymbol{0} & \boldsymbol{0} \\ \boldsymbol{0} & \boldsymbol{0} & \boldsymbol{B}_m^u & \boldsymbol{B}_m^{\theta z} \end{bmatrix} \tag{4.35}$$

$$\boldsymbol{\beta} = \begin{bmatrix} \boldsymbol{\beta}_s \\ \boldsymbol{\beta}_b \\ \boldsymbol{\beta}_m \end{bmatrix}, \quad \boldsymbol{q} = \begin{bmatrix} \boldsymbol{q}_w \\ \boldsymbol{q}_\theta \\ \boldsymbol{q}_u \\ \boldsymbol{q}_{\theta z} \end{bmatrix} \tag{4.36}$$

where $\boldsymbol{r}_u$, $\boldsymbol{r}_w$ and $\boldsymbol{r}_\theta$ are the element nodal (generalized) forces and

$$\mathbf{H}_s^s = \int_{\Omega_e} \mathbf{P}_s^{\mathrm{T}} \mathbf{C}_s^{-1} \mathbf{P}_s \mathrm{d}\Omega, \quad \mathbf{H}_s^b = \int_{\Omega_e} \mathbf{P}_{bs}^{\mathrm{T}} \mathbf{C}_b^{-1} \mathbf{P}_{bs} \mathrm{d}\Omega \tag{4.37a}$$

$$\mathbf{H}_{bs}^b = \int_{\Omega_e} \mathbf{P}_{bs}^{\mathrm{T}} \mathbf{C}_b^{-1} \mathbf{P}_b \mathrm{d}\Omega, \quad \mathbf{H}_b^b = \int_{\Omega_e} \mathbf{P}_b^{\mathrm{T}} \mathbf{C}_b^{-1} \mathbf{P}_b \mathrm{d}\Omega \tag{4.37b}$$

$$\boldsymbol{B}_s^w = \int_{\Omega_e} \mathbf{P}_s^{\mathrm{T}} \mathbf{D}_s \mathbf{U}_w \mathrm{d}\Omega, \quad \boldsymbol{B}_{bs}^\theta = \int_{\Omega_e} \mathbf{P}_{bs}^{\mathrm{T}} \mathbf{D}_b \mathbf{U}_\theta \mathrm{d}\Omega, \tag{4.37c}$$

$$\boldsymbol{B}_s^{w\theta} = \int_{\Omega_e} \mathbf{P}_s^{\mathrm{T}} \mathbf{D}_s^{\mathrm{T}} \bar{\mathbf{L}} \mathrm{d}\Omega, \quad \boldsymbol{B}_b^\theta = \int_{\Omega_e} \mathbf{P}_b^{\mathrm{T}} \mathbf{D}_b \mathbf{U}_\theta \mathrm{d}\Omega \tag{4.37d}$$

$$\boldsymbol{B}_s^\theta = \int_{\Omega_e} \mathbf{P}_s^{\mathrm{T}} \mathbf{U}_\theta \mathrm{d}\Omega \tag{4.37e}$$

$$\boldsymbol{B}_m^{\theta z} = \int_{\Omega_e} \mathbf{P}_m^{\mathrm{T}} \mathbf{D}_m \hat{\mathbf{L}} \mathrm{d}\Omega, \quad \boldsymbol{B}_m^u = \int_{\Omega_e} \mathbf{P}_m^{\mathrm{T}} \mathbf{D}_m \mathbf{U}_u \mathrm{d}\Omega, \tag{4.37f}$$

Matrices $\mathbf{H}_s^b$, $\mathbf{H}_{bs}^b$ and $\mathbf{B}_{bs}^\theta$ reflect the effect of coupling on the stress approximation, while matrix $\mathbf{B}_s^{w\theta}$ reflects the effect of linking on the displacement interpolation. Notice that depending on the purpose of the analysis, the shear energy can be arbitrarily excluded by simply putting $\mathbf{H}_s^s = \mathbf{0}$ and this does not result in any ill-conditioning of the problem. The integration of all the above terms is performed numerically.

The fully integration scheme is adopted, but the Gauss quadrature would be adopted in order only to reduce the computational cost being, the element, free of locking.

Operating within the hybrid stress formulation described in the previous section, the attention is focused here on constructing a quadrilateral 4-node element with the features discussed in Section 1. In particular, the representations assumed for geometry, generalized displacements and generalized stresses are discussed in detail. Reference is made to the typical element Ω_e. Based on Equation (**??**), generalized displacements are required to be continuous across element boundaries and stress resultants are required to satisfy the equilibrium equations within each element. Notice that discontinuities in stress resultants across element boundaries are permitted.

4.6 Element reference configurations

The four node shell element is described by the local $(x; y; z)$ co–ordinate whose origin is defined at the geometric center of the element. The geometric center of the element is determined by using the given global co–ordinates of the element nodes:

$$\boldsymbol{X}_c = \frac{1}{4} \sum_{i=1}^{4} \boldsymbol{X}_i \qquad (4.38)$$

where $\boldsymbol{X}_c$ are the global co-ordinates of the center of the element

and $\boldsymbol{X}_i$ are the global co–ordinates of node i. The local co–ordinate system $(x; y; z)$ is defined by first determining the vectors passing through the opposite midpoints of the shell mid–surface, $\boldsymbol{i}_1$ and $\boldsymbol{i}_2$:

$$\boldsymbol{X}_{\text{side } i} = (\boldsymbol{X}_i + \boldsymbol{X}_{i+1})/2 \tag{4.39}$$

$$\boldsymbol{i}_1 = \frac{\boldsymbol{X}_{\text{side } 2} - \boldsymbol{X}_{\text{side } 4}}{\| \boldsymbol{X}_{\text{side } 2} - \boldsymbol{X}_{\text{side } 4} \|} \qquad \boldsymbol{i}_2 = \frac{\boldsymbol{X}_{\text{side } 3} - \boldsymbol{X}_{\text{side } 1}}{\| \boldsymbol{X}_{\text{side } 3} - \boldsymbol{X}_{\text{side } 1} \|} \tag{4.40}$$

The local co–ordinate vectors $\boldsymbol{i}_x, \boldsymbol{i}_y, \boldsymbol{i}_z$ are found by

$$\boldsymbol{i}_z = \boldsymbol{i}_1 \wedge \boldsymbol{i}_2 \qquad \boldsymbol{i}_y = \frac{(\boldsymbol{i}_z \wedge \boldsymbol{i}_1) + \boldsymbol{i}_2}{\| (\boldsymbol{i}_z \wedge \boldsymbol{i}_1) + \boldsymbol{i}_2 \|} \qquad \boldsymbol{i}_x = \boldsymbol{i}_y \wedge \boldsymbol{i}_z \tag{4.41}$$

in which $\boldsymbol{i}_2$ direction was summed in the derivation of $\boldsymbol{i}_y$ in order to get equal angle between $\boldsymbol{i}_2$, $\boldsymbol{i}_y$ and between $\boldsymbol{i}_x$, $\boldsymbol{i}_i$.

And the local co–ordinate of the node i are

$$\boldsymbol{x}_i = \begin{bmatrix} \boldsymbol{i}_x & \boldsymbol{i}_y & \boldsymbol{i}_z \end{bmatrix}^T (\boldsymbol{X}_i - \boldsymbol{X}_c) = \boldsymbol{E}_0(\boldsymbol{X}_i - \boldsymbol{X}_c) \tag{4.42}$$

Having defined the local co-ordinate base vectors, the transformation of the displacement parameters $\boldsymbol{u}_i$, $\boldsymbol{\phi}_i$ at node i from the element local co–ordinates, to the global co–ordinates, is performed in a standard way such that

$$
\begin{bmatrix} \boldsymbol{u} \\ \boldsymbol{\phi} \end{bmatrix}_i = \begin{bmatrix} u_i \\ v_i \\ w_i \\ \phi_{xi} \\ \phi_{yi} \\ \phi_{xi} \end{bmatrix} = \begin{bmatrix} \boldsymbol{E}_0 & \boldsymbol{0} \\ \boldsymbol{0} & \boldsymbol{E}_0 \end{bmatrix} \begin{bmatrix} U_i \\ V_i \\ W_i \\ \theta_{Xi} \\ \theta_{Yi} \\ \theta_{Zi} \end{bmatrix} = \boldsymbol{E}_{0i} \begin{bmatrix} \boldsymbol{U} \\ \boldsymbol{\theta} \end{bmatrix}_i \qquad (4.43)
$$

4.7 Some remarks

The developed finite element has been checked (see the numerical tests in Section **??**) to be locking-free and pass all the patch tests (design criteria 2 and 3 in Section **??**). It is interesting to underline that the key steps to reach this goal are: linking the displacement interpolation and making the stress approximation locally equilibrated. Both these steps are actually necessary. In fact, either using the equilibrated stress approximation (4.31) together with the standard 4-node displacement interpolation or the linked displacement interpolation (**??**) together with a non-equilibrating stress approximation results in an element that, although stable, fails to pass all the patch tests. This can be explained by recalling that if the assumed stresses are equilibrated within each element, then the assumed displacements actually play their role only on the element boundaries (see functional (**??**) or matrices G in Equations (4.37c) and (**??**)). On the other hand, the linked interpolation

guarantees kinematic consistency on the element boundaries, since the associated shear strains are constant along each element side.

Chapter 5

Nonlinear flat shell model

The development of finite element models for non-linear analysis of shells has always presented a major challenge due to the theoretical intricacies involved. Furthermore, an added impetus is the rapidly growing industrial need for such general shell models to perform large-scale computations in important applications, such as sheet forming processes and progressive failure analysis of composite shell structures.

5.1   Linear strain in local modeling

As stated in Section 3.1 we need a linear strain in the corotational frame in order to obtaine the non–linear model. In this case is possible to completely reuse the linear strain assumed in equations 4.2 for the continous model.

In particular, we need to cast the linear strain energy of the shell model **??** in the corotational framework **??** in order to obtain the variations in a general way only by variation of the nodal displacements.

For this porpoise the linear strain energy of the flat–shell element need to be manipulating for reordering the local variable with respect to the global ones. By using energetic equivalence it is possible to simple reorder the local variable in order to use it in the corotational framework:

$$\boldsymbol{\beta}^T \boldsymbol{B} \boldsymbol{q} = \boldsymbol{\beta}^T \boldsymbol{Q} \boldsymbol{g}[d_e] \tag{5.1}$$

Now, it is possible to use the $\boldsymbol{H}$ and the $\boldsymbol{Q}$ in the corotational framework with the fulfillment of the objectivity requiring. The full nonlinear element it is obtained then by rotating the global displacements and rotations in the local corotational frame:

$$\boldsymbol{g}_{ei} = \begin{bmatrix} \boldsymbol{d}_{ci} \\ \boldsymbol{\varphi}_{ci} \end{bmatrix} = \begin{bmatrix} \boldsymbol{Q}[\boldsymbol{\alpha}]^T (\boldsymbol{X}_i + \boldsymbol{d}_i) - \boldsymbol{X}_i \\ \log(\boldsymbol{Q}[\boldsymbol{\alpha}]^T \boldsymbol{R}[\boldsymbol{\varphi}_i]) \end{bmatrix} \tag{5.2}$$

in which $i = 1 \cdots 4$ the node number and $\boldsymbol{\alpha}$ means an average element rotation. The successive variations can be performed automatically by an algebraic manipulator or symbolically. In any cases it is more convenient to perform the variation before to define $\boldsymbol{\alpha}$.

5.2 Corotational reference configurations

A suitable choice for the average rotation matrix may be obtained simply letting:

$$\boldsymbol{\alpha}_e = \frac{1}{4} \sum_{k=1}^{4} \boldsymbol{\varphi}_c^{(k)}, \quad \boldsymbol{Q} = \log \boldsymbol{\alpha}_e \tag{5.3}$$

Using this definition it is possible to perform the successive variation of the $\boldsymbol{Q}$ matrix in order to obtain complete informations that needs for the nonlinear formulation.

Letting $\boldsymbol{\alpha}_{e1} = \frac{1}{4} \sum_{k=1}^{4} \boldsymbol{\varphi}_{c1}^{(k)}$ being $\boldsymbol{\alpha}_e$ linearly dependent of the global rotations, for our chose, then the first variation of $\boldsymbol{Q}$ become simply:

$$\boldsymbol{Q}_1 = \boldsymbol{W}[\boldsymbol{\alpha}_{e1}] \tag{5.4}$$

this allows to get the nodal variations coherent until fourth order by the corotational asymptotic framework developed in Section **??**.

In order to complete all tool needing for evaluate vectors and matrix quantity in the corotational asymptotic framework we need to define $\boldsymbol{G}$, $\boldsymbol{G}_2$ and $\boldsymbol{r}$ operators for the flat shell nonlinear element.

Chapter 6

Numerical results

In order to show capability of the ANM a lot of results are reported in comparison with the ABAQUS and, when possible, with the HC finite element programs. The ABAQUS results were product by a general static solver using Riks's nonlinear algorithm and the S4-R or the S8-R shell elements [?], respectively 4 and 8–Noded, in wich the last one showed very good performance also for coarse mesh but it is quite computationally expensive in case of very fine mesh and high number of dofs. Conversely, S4-R showed quite good convergence for fine mesh. With the HC element we refer to the high continuity finite elements for Kirchhoff's plate in a ANM framework [?, ?] that showed very good performance also for coarse mesh with some limits when out–plane shear deformation become important. Also, some results were compared with very popular benchmarks presents in literature.

Firstly, some simple test with analytical or numerical solution very known also in post–buckling range, such as Eulero's beam, Roorda's beam, shallow arch (that showed purely flexural behavior), share plate (with purely shear), cantilever beam, L-frame beam (that mixing shear and flexural) were reported in order to show accuracy of CR-4 element in ANM context. Obviously, pure flexural test were modeled using only one element in the width.

In succession, some structure beam–like with the geometrical hypothesis of cylindrical solid, simply or multi connected were studied because that is a fundamental structure in all the fields of civil and industrial engineering, in particular thin walled open sections beams such as: T C Z and Cross–section. Finally, some general shell and also a stiffened girder study were reported.

6.1   Eulero beam

The first example taken in consideration the simple case of a planar beam under compression as in section **??**. For this simple test we reported the convergence of the lowest buckling load in comparison with HC, S4-R and S8-R elements, and in the equilibrium paths. We can note a very good rate of convergence for CR4 element in the predicting buckling load and also a very good behavior in the reconstruction of equilibrium path also in post–buckling range.

For this simple example, the nonlinear behavior of flexural and membrane modeling of the CR-4 element can be investigate separately by constraining the structure to buckle in plane or out of plane. The results of both case are reported separately in the next two sections.

6.1.1 Eulero beam out–plane

In this case only flexural behavior are activate during buckling and post–buckling. Material and geometrical data are $E = 4.8e6$, $\nu = 0.3$, $t = 0.1$, $b = 1$ and $L = 20$. As reported in table 6.1 CR-4 element presents very good rate of convergence in case of buckling load. . The equilibrium path for w_a, out–plane displacement in the middle span is reported in the figure 6.1 that shows very high accuracy for CR-4 element also for very large displacements near $0.5L$.

	el.n	HC	S4-R	S8-R	CR4
	16	9.901	9.9330	9.8685	9.8942
λ_b	32	9.877	9.8850	9.8684	9.8699
	64	9.872	9.8730	9.8684	9.8632

Table 6.1 Euler beam out–plane: fem convergence
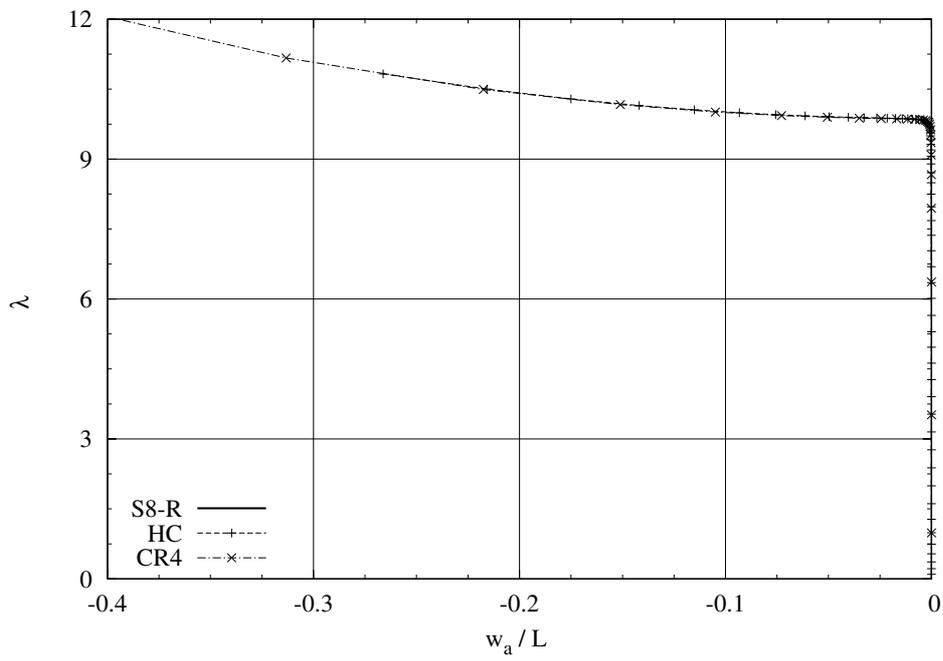
Figure 6.1 Euler beam out–plane: equilibrium path

6.1.2   Eulero beam in–plane

As already done for flexural behavior, it is possible, for this simple test, investigate only the nonlinear membrane part of the CR-4 element model by constraint the structure to buckle in plane. The geometry and material data are $E = 6.0e5$, $\nu = 0.0$, $t = 1.0$, $b = 0.2$ and $L = 20$. In this case, CR-4 showed poor performance in case of coarse mesh, but already good behavior in case of fine mesh. To be noted that also in the case of coarse mesh, CR-4 performs better than S4-R that predict 3 times higher buckling load for the coarse mesh. The in–plane displacement component v_a is reported in figure **??** and exploit good performance of CR-4 element. To be noted that in all the cases where used only 3 elements in the width, and the mesh refinement was in the x direction.

	el.n	HC	S4-R	S8-R	CR4
	16	9.918	33.380	9.8676	9.9314
λ_b	32	9.870	14.964	9.8669	9.8835
	64	9.870	10.326	9.8668	9.8716

Table 6.2 Euler beam in–plane: fem convergence

6.2   Roorda frame
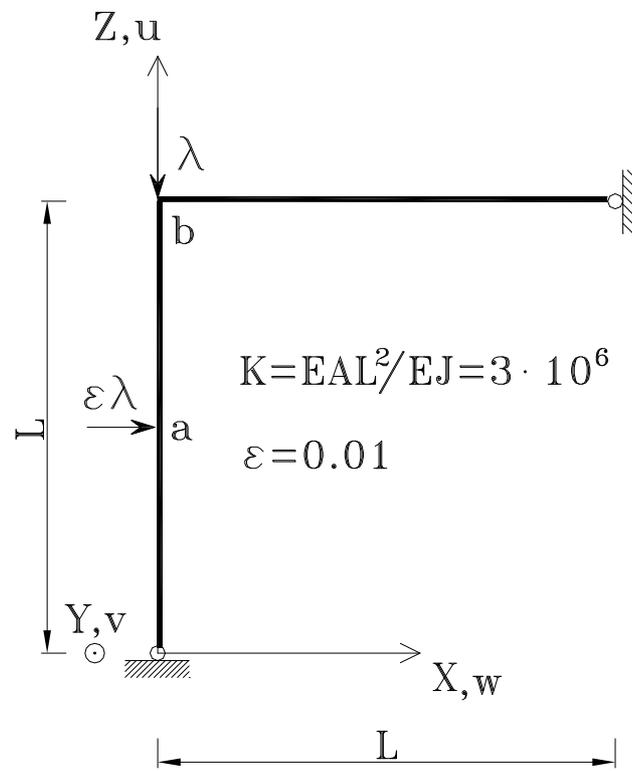
Figure 6.2 Roorda frame
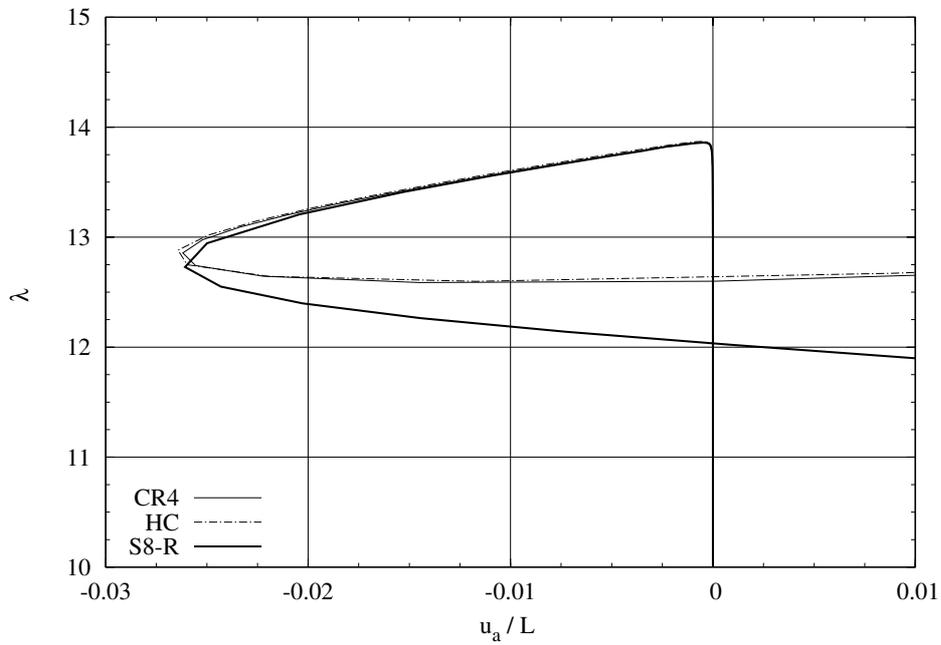
Figure 6.3 Roorda frame: equilibrium path

	el.n	HC	S4-R	S8-R	beam	CR4
	16	13.954	14.005	13.886		13.937
λ_b	32	13.903	13.915	13.885	13.886	13.898
	64	13.890	13.893	13.884		13.888

Table 6.3 Roorda frame: fem convergence

6.3   Flexural-Torsional beam

The simple case of flexural-torsional buckling were investigate in a structure such as reported in fig. **??**. The buckling load convergence is reported in tab. **??**.
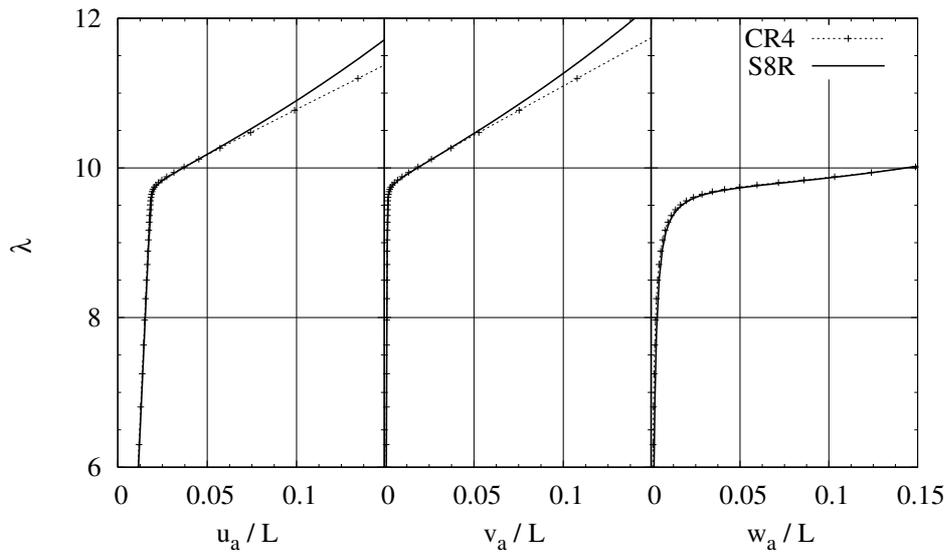
Figure 6.4 Flexural-Torsional beam: equilibrium path

6.4 Shear plate

A simply supported rectangular plate submitted to pure shear discretized with regular mesh were analyzed. The geometry and material data is reported in fig. 6.5. The results obtained fo the geometric ratios $a/b = 1.0$ and $a/b = 1.5$ are reported in tab. 6.4 where we can see a good performance of CR4 element in the prediction of first buckling load. For the the first case the analytical result is 000.00 [**?**]. In fig. **??** the equilibrium path for the case $a/b = 1.5$ is compared with the reference solution and normalized respect to the plate thickness.

In [33] sono riportati i risultati ottenuti con ANM per lo stesso test. vedere anche **??**

In fig. **??** the first buckling mode for $a/b = 1.5$.
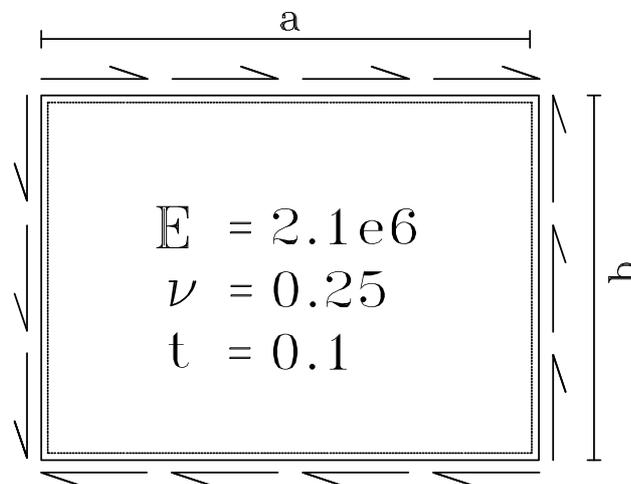
Figure 6.5 Shear plate: geometry and loads

	n.elem.	HC	*S4-R*	*S8-R*	*CR4*
a/b=1	9x9	173.2	186.7	170.6	182.05
	27x27	172.2	172.5	170.2	171.90
	81x81	171.8	170.6	170.2	171.06
a/b=1.5	9x18	132.08	139.0	129.53	138.84
	27x54	130.52	130.69	129.46	130.53
	81x162	130.28	129.63	129.46	*

Table 6.4 Shear plate: fem convergence
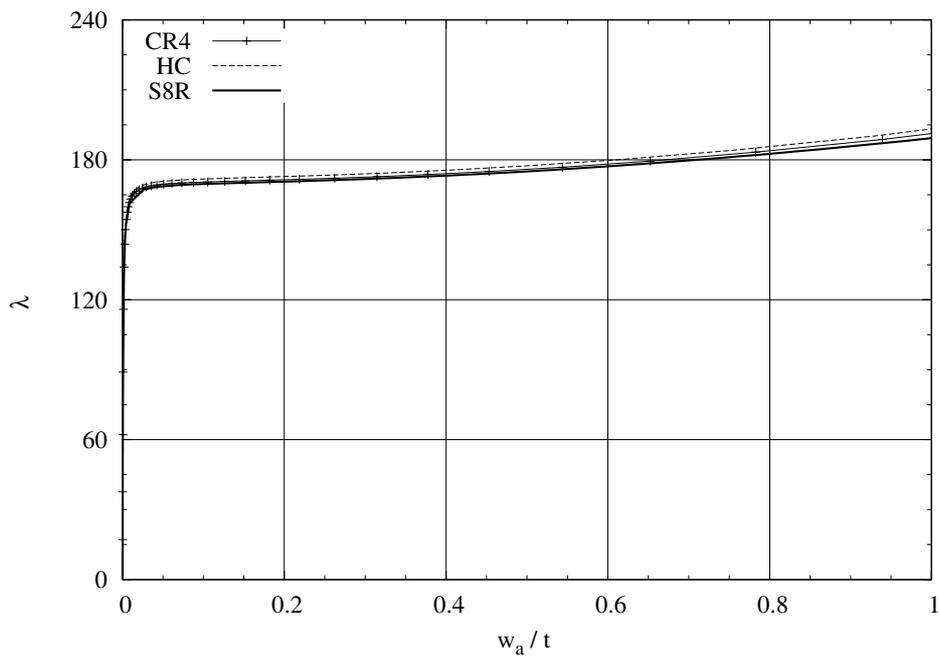
Figure 6.6 Shear plate: equilibrium paths $a/b = 1.0$
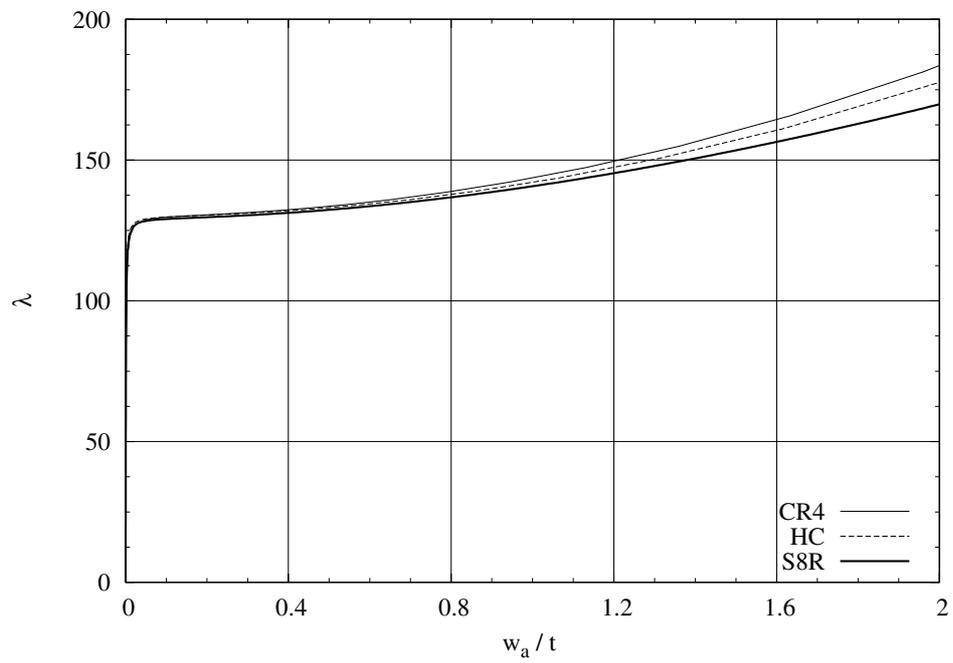
Figure 6.7 Shear plate: equilibrium paths $a/b = 1.5$
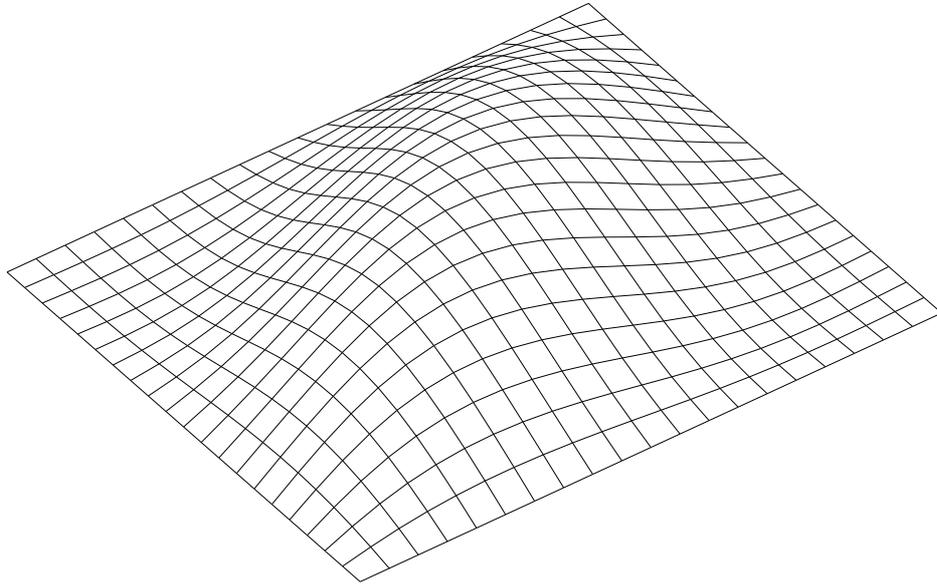
Figure 6.8 Shear plate: buckling $a/b = 1.0$
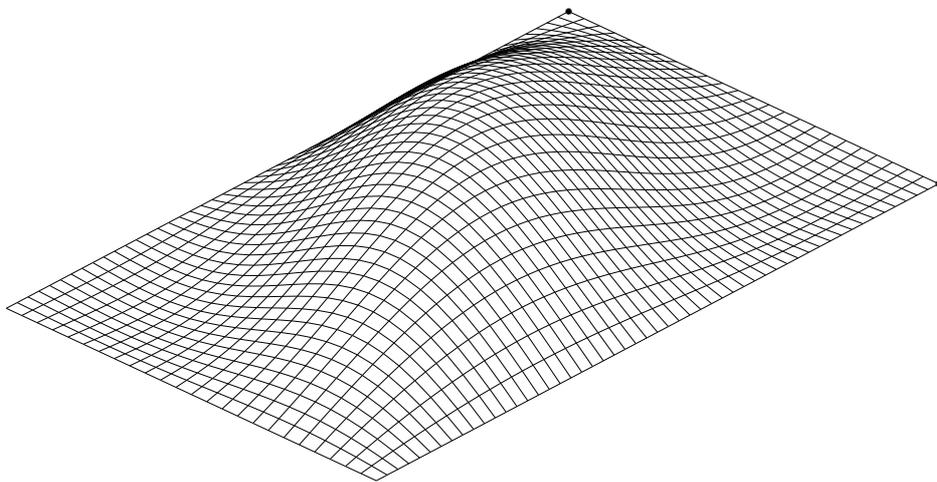
Figure 6.9 Shear plate: buckling $a/b = 1.5$

6.5   L-shaped frame

The L-shaped beam is considered in this test [34]. Geometry and ma-
terial are the same of in fig. **??**. The structure is discretized with 2
element in the width ad 8 for each brace. Refined mesh is applied by
splitting each element regularly in 4 elements. The convergence of the
lowest buckling load is reported in tab. **??** and the equilibrium path
for CR-4 compared with ABAQUS coverged solution is depicted in fig.
6.10. The agreement between path-following and asymptotic numeri-
cal methods it is evident for a large displacement range of $0.2L$ within
an acceptable error.
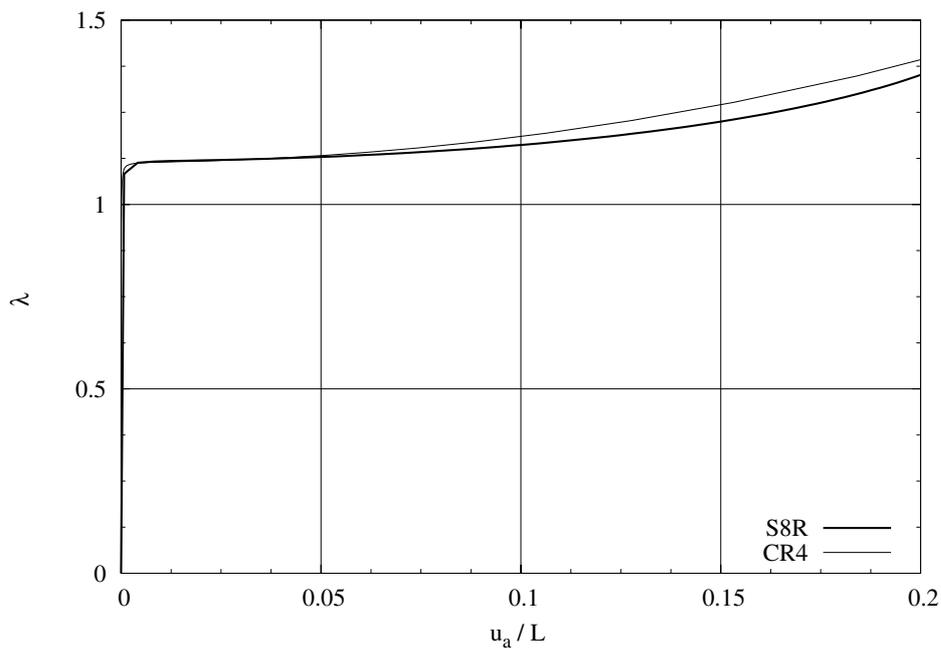
Figure 6.10 L-shaped frame: equilibrium path

6.6   Cross–section beam

$$\begin{aligned} E &= 2.1\,e4 \\ \nu &= 0.3 \\ \varepsilon &= 0.001 \end{aligned}$$

$L = 100$
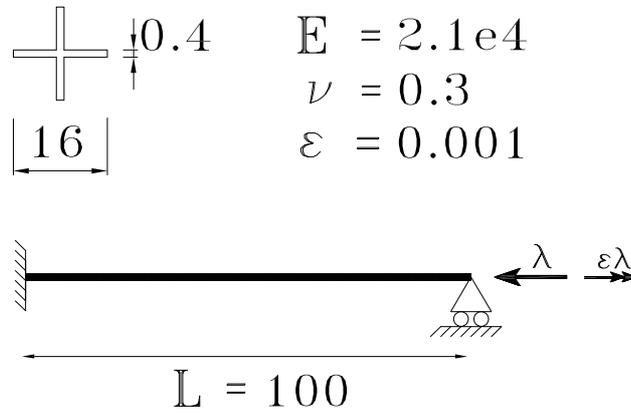
Figure 6.11 Cross–section beam

	HC	*CR4* coarse	*CR4* fine
λ_1	2.5923e2	2.4780e2	2.5257e2
λ_2	2.6742e2	2.6093e2	2.6521e2
λ_3	2.8418e2	2.8370e2	2.8644e2

Table 6.5 Cross-Section: fem convergence
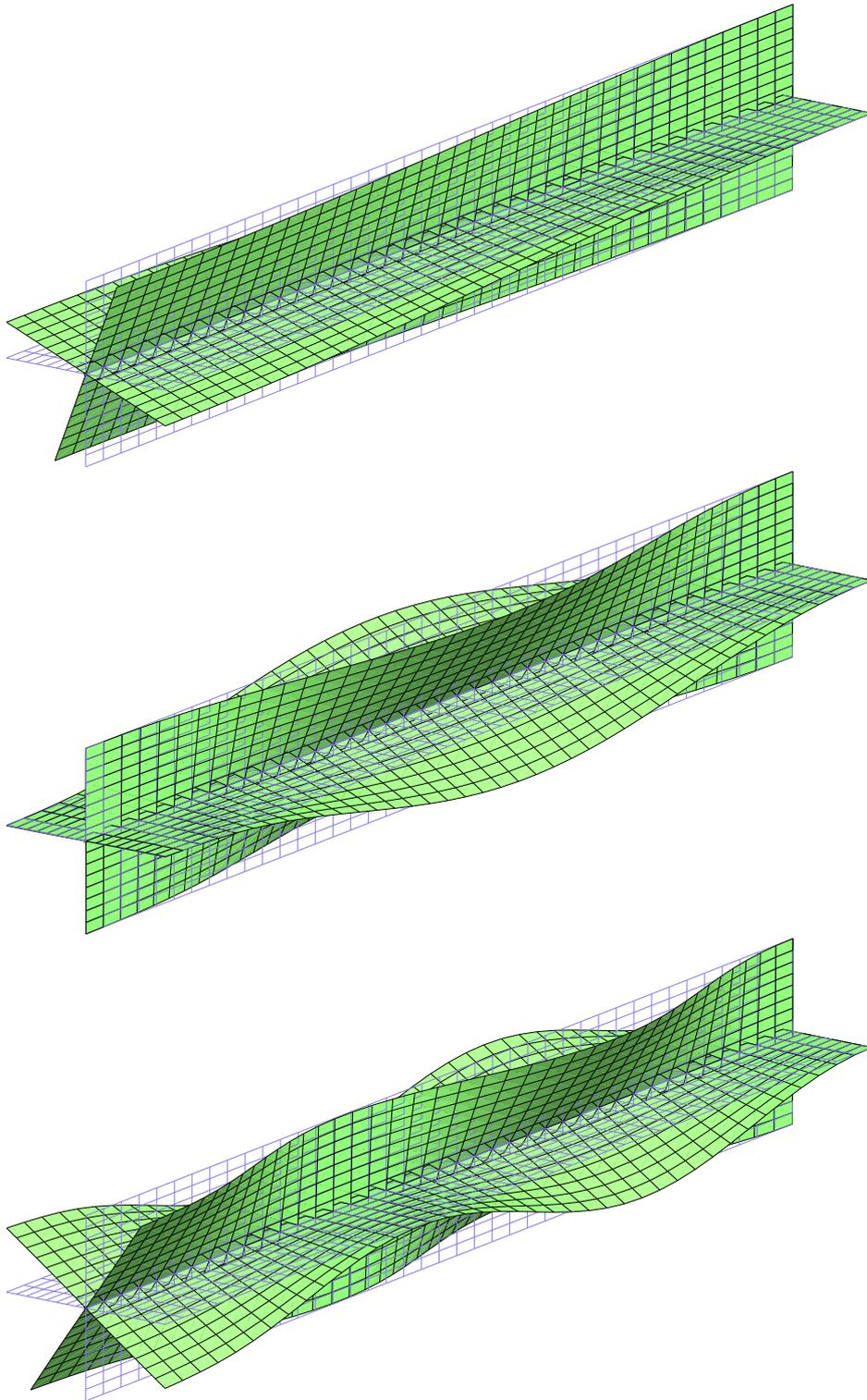
Figure 6.12 Cross–section: lowests buckling modes

6.7 C–section beam
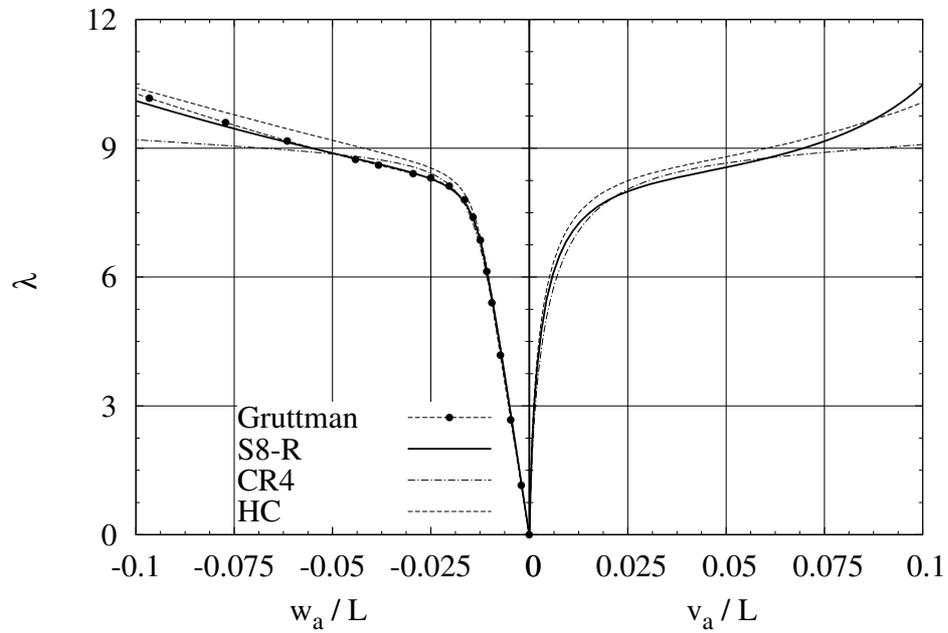
Figure 6.13 C–section beam symmetric

6.8 T-section beam
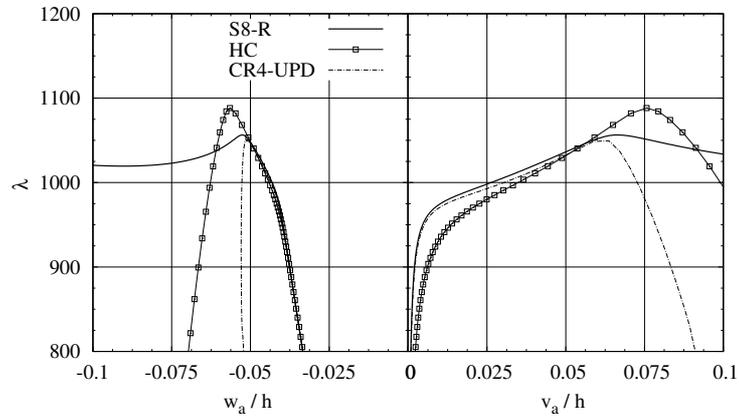
Figure 6.14 T–section beam L=750: equilibrium paths
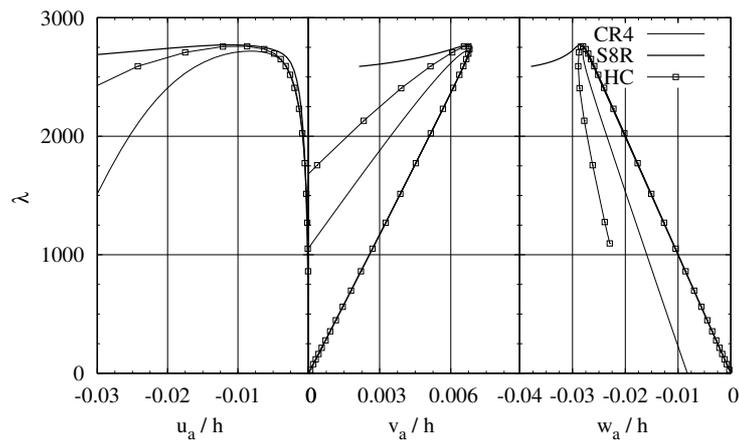
Figure 6.15 T–section beam L=450: equilibrium paths

6.9   Z-section cantilever

$\mathbb{E}$ = 2.0e5
ν = 0.3
ε = 0.001
h = 142.88
b = 85.73
t = 12.7

$\mathbb{L}$ = 100
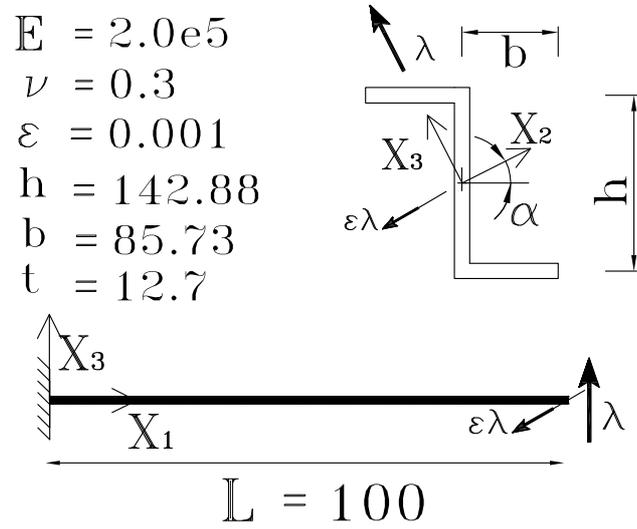
Figure 6.16 Z–section cantilever
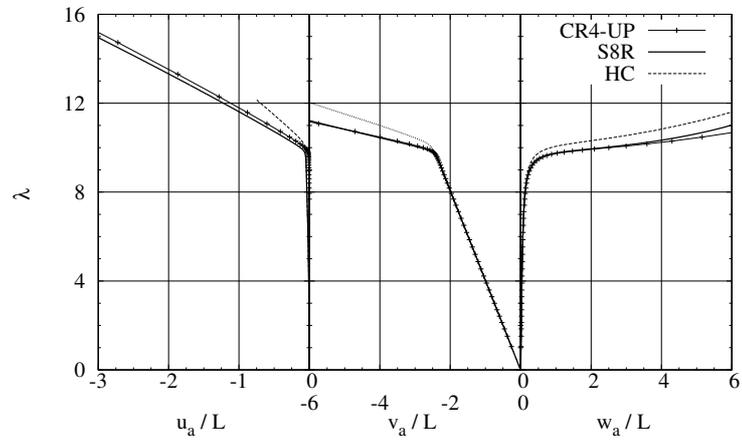
Figure 6.17 Z–section cantilever-paths
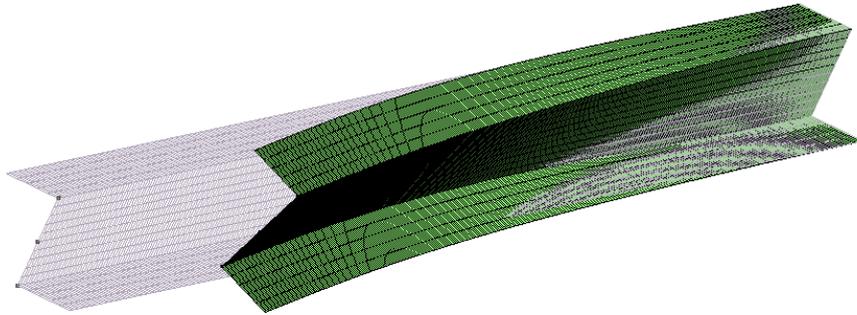
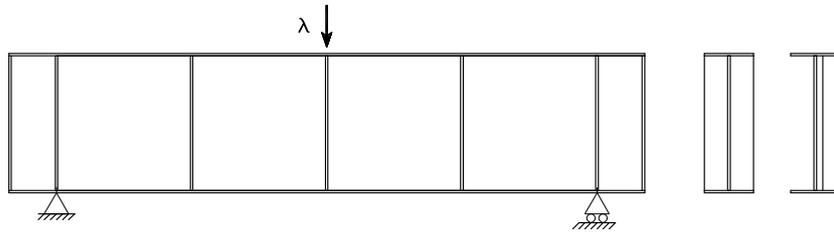**Figure 6.18** Z–section cantilever: lowests buckling modes

6.10   Stiffened girder

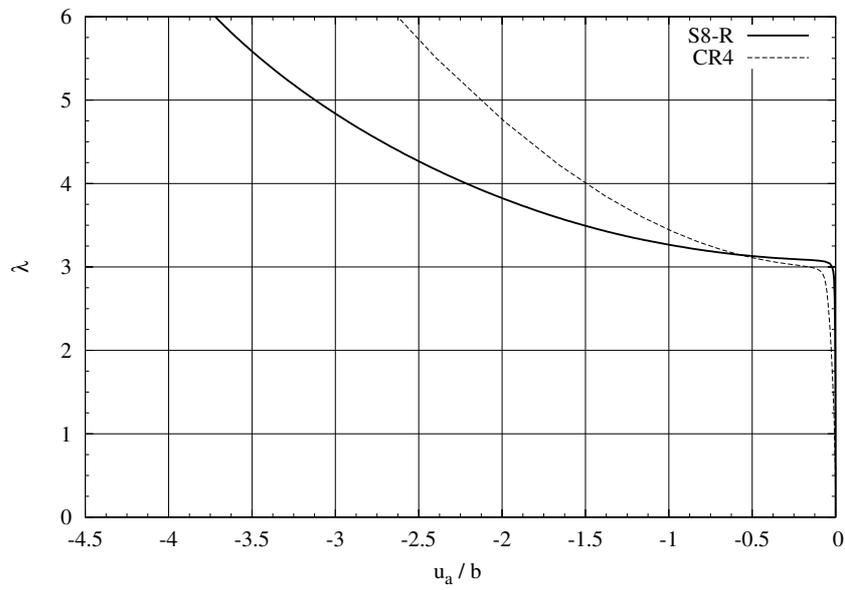**Figure 6.19** Stiffened girder

Figure 6.20 Stiffened girder: equilibrium path

Chapter 7

Concluding remarks

The paper presents a corotational formulation, suitable for a nonlinear, fourth–order accurate asymptotic postbuckling analysis of structures exploiting three dimensional finite rotations. Its FEM implementation is discussed in detail, and basic expressions for recovering the first four strain energy variations are given. The approach allows a geometrically coherent, locking–free, nonlinear modeling to be obtained, starting from a standard, linear or simplified nonlinear, finite element local discretization, thus overcoming, in a simple way, the main difficulty in the implementation of the asymptotic analysis, that is the use of fourth–order accurate kinematics. Although complex algebra is necessary in the derivation of the strain energy derivatives in an explicit form, it could be noticeably simplified by the use of algebraic manipulators, see [**?**].

The proposed approach is fully implemented, by deriving the relevant terms of the energy expansion, for the case of 3D Reissner beam assemblages. This structural typology was chosen as the simplest tutorial, but also because it is characterized by a weak postbuckling stress redistribution and therefore highly sensitive to kinematical coherency. In this way it is particularly suitable for testing the overall reliability of the approach. The extension to other structural typologies, such as plates or shells, only requires an appropriate definition of the corotational rotation α in terms of the element displacement parameters. For elements with rotational degrees of freedom, a possible choice could be to directly refer to their average, as done for the beam element. The derivations of the energy expressions in an explicit form is straightforward and can be easily performed through algebraic manipulators [**?**]. Improvements in the beam modeling are also possible by the use of refined models,such as the one derived in [**?**] from Saint Venànt's rods theory. This implies simple changes in the expression of the complementary energy of the element only affecting the local FEM model and could be useful for improving accuracy in the case of thin–walled or complex sections (at least in these cases, where local buckling produced by in-plane distortions of the section can be neglected [**?**, **?**]).

It is worth mentioning that the mixed format, in displacement and stress variables, used in the local finite element discretization, is an important part of the proposed approach. It allows for noticeable sim-

plifications in the algebra of energy derivatives and also plays an important role in the robustness and reliability of the asymptotic analysis by avoiding the so called extrapolation locking phenomena [**?**]. The solution of eqs. (2.3), (2.4) and (2.7) can be conveniently performed by means of a static condensation of stress variables at the element level within a pseudo–compatible solution scheme. This implies a minimal computational extra–cost with respect to a compatible modeling using displacement variables alone, while maintaining all the advantages of the mixed formulation (see [**?**] for detail).

The use of quadratic kinematics for the local FEM modeling instead of the linear one is only related to best–compromise choices, as it introduces slightly more complex expressions and the same improvement in accuracy can be achieved by refined meshes. Numerical results, referring to a selection of benchmark tests, show fast convergence at mesh refining and great accuracy, for both these choices, even in cases of complex coupled multimodal bucklings.

Bibliography

[1] Riks, E. *Computer Methods in Applied Mechanics and Engineering* **136**(1-2), 59–92 September (1996).

[2] Riks, E. *International Journal of Solids and Structures* **15**(7), 529–551 (1979).

[3] Crisfield, M. A. *Non-linear Finite Element Analysis of Solids and Structures.*, volume 1. (1991).

[4] Koiter, W. T. *On the stability of elastic equilibrium.* PhD thesis, (1945).

[5] Lanzo, A. D., Garcea, G., and Casciaro, R. *International Journal of Numerical Methods in Engineering* **38**(14), 2325–2345 (1995).

[6] Casciaro, R., Garcea, G., Attanasio, G., and Giordano, F. *Computers and Structures* **66**(5), 585–595 (1998).

[7] Salerno, G. and Casciaro, R. *International Journal of Numerical Methods in Engineering* **40**(5), 833–861 (1997).

[8] Salerno, G. and Uva, G. *International Journal of Non-Linear Mechanics* **41**(3), 359–376 (2006).

[9] Casciaro, R. and Mancusi, G. *International Journal of Numerical Methods in Engineering* **67**(6), 815–840 (2006).

[10] Casciaro, R. *Phenomenological and Mathematical Modelling in Structural Instabilities* (2005).

[11] Lanzo, A. D. and Garcea, G. *International Journal of Numerical Methods in Engineering* **39**(17), 3007–3031 (1996).

[12] Rankin, C. C. and Omid, B. N. *Computers and Structures* **30**(1-2), 257–267 (1988).

[13] Rankin, C. C., Brogan, F. A., and Riks, E. *Computational Mechanics* **13**(3), 143–156 December (1993).

[14] Garcea, G., Madeo, A., Zagari, G., and Casciaro, R. *International Journal of Solids and Structures* **46**(2), 377–397 January (2009).

[15] Garcea, G., Salerno, G., and Casciaro, R. *Computer Methods in Applied Mechanics and Engineering* **180**(1-2), 137–167 (1999).

[16] Garcea, G. *Computer Methods in Applied Mechanics and Engineering* **180**(1-2), 137–167 November (1999).

[17] Garcea, G., Trunfio, G. A., and Casciaro, R. *International Journal of Numerical Methods in Engineering* **55**(1), 73–100 (2002).

[18] Casciaro, R., Salerno, G., and Lanzo, A. D. *International Journal of Numerical Methods in Engineering* **35**, 1397–1426 (1992).

[19] Casciaro, R. *Computers & Structures* **66**(5), 585–595 March (1998).

[20] Garcea, G. *Computer Methods in Applied Mechanics and Engineering* **190**(26-27), 3369–3399 (2001).

[21] Carnoy, E. *Computer Methods in Applied Mechanics and Engineering* **23**(2), 143–174 (1980).

[22] Flores, F. G. and Godoy, L. A. *International Journal of Numerical Methods in Engineering* **33**, 1775–1794 (1992).

[23] Pacoste, C. *Computer Methods in Applied Mechanics and Engineering* **125**(1-4), 319–343 September (1995).

[24] Wu, B. and Wang, Z. *Computer Methods in Applied Mechanics and Engineering* **145**(3-4), 203–215 (1997).

[25] Poulsen, P. N. and Damkilde, L. *International Journal of Numerical Methods in Engineering* **42**(4), 685–702 (1998).

[26] Abichou, H., Zahrouni, H., and Ferry, M. P. *Computer Methods in Applied Mechanics and Engineering* **191**(51-52), 5795–5810 (2002).

[27] Boutyour, E. H., Zahrouni, H., Ferry, M. P., and Boudi, M. *Journal of Computational and Applied Mathematics* **168**(1-2), 77–85 (2004).

[28] Schafer, B. W. and Brady, L. G. *International Journal of Structural Stability and Dynamics* **6**(3), 333–358 (2006).

[29] Chen, H. and Virgin, L. N. *International Journal of Solids and Structures* **43**(13), 3983–4007 (2006).

[30] Aminpour, M. A. *International Journal of Numerical Methods in Engineering* **33**(1), 19–38 (1992).

[31] Duan, M. and Miyamoto, Y. *Journal of Engineering Mechanics* **128**(2), 202–208 (2002).

[32] de Miranda, S. and Ubertini, F. *International Journal of Numerical Methods in Engineering* **65**(6), 808–833 (2006).

[33] Vannucci, P., Cochelin, B., Damil, N., and Ferry, M. P. *International Journal of Numerical Methods in Engineering* **41**(8), 1365–1389 (1998).

[34] Crisfield, M. *Computer Methods in Applied Mechanics and Engineering* **81**(2), 131–150 August (1990).